Sustainable Cities and Society 153 (2026) 108122



Contents lists available at ScienceDirect

Sustainable Cities and Society

journal homepage: www.elsevier.com/locate/scs



Two decades of urban surface heat dynamics in Gujarat, India: long-term trends and environmental associations

Yagni Rami [a,*], TC Chakraborty [b]

[a] Environmental Engineering Department, L D College of Engineering, Ahmedabad, Gujarat, 380015, India
[b] Earth System Modeling Group, Pacific Northwest National Laboratory (PNNL), Richland, WA, 99354, United States

ARTICLE INFO

Keywords:
Land surface temperature (LST)
Surface urban heat island (SUHI)
Remote sensing
Explainable artificial intelligence
Urban climate
Heat mitigation
Gujarat

ABSTRACT

Rapid urbanization and regional warming have intensified urban climate stress across India. Here, we assess thermal, atmospheric, and land-surface dynamics across five major and rapidly growing cities in Gujarat, namely Ahmedabad, Gandhinagar, Vadodara, Surat, and Rajkot, during 2000–2024. Using satellite-derived LST, SUHI, AOD, NDVI, NDBI, and surface albedo, we quantified long-term warming trends, urban–rural environmental contrasts, and land-surface transformation.

Daytime LST declined across the five cities, whereas nighttime LST increased, with statistically significant trends in four cities. Nighttime LST increased significantly in four cities, whereas nighttime SUHI intensified significantly only in Vadodara, suggesting that absolute surface warming does not necessarily translate into increasing urban–rural thermal contrasts. Urban–rural analyses showed persistent vegetation deficits, with mean ΔNDVI ranging from −0.079 in Gandhinagar to −0.171 in Surat, while built-up contrasts reached ΔNDBI = 0.085 in Surat. AOD exhibited increasing trends across all five cities, indicating increasing aerosol loading over the study period. SHAP analysis identified urban–rural vegetation differences (ΔNDVI) and built-up differences (ΔNDBI) as prominent predictors of daytime SUHI variability, while aerosol loading and albedo showed comparatively smaller contributions in most cities, with notable city-specific exceptions in Rajkot and Surat. These relative contributions represent model-dependent predictive attributions and may reflect shared information among correlated predictors. Given the limited temporal and cross-city predictive performance, the SHAP results are interpreted as exploratory, model-dependent associations within the five study cities rather than generalizable or causal environmental relationships.

Overall, vegetation and built-up contrasts were statistically associated with urban thermal variability across the study cities, although their relative importance varied by city and time of day. These associations support consideration of urban greening, vegetation conservation, and impervious-surface management in thermal-resilience planning; however, the effectiveness of specific interventions cannot be established from predictive attribution analysis alone. Furthermore, the 1-km spatial resolution of MODIS LST limits the representation of fine-scale urban thermal heterogeneity and local microclimatic conditions. The analysis characterizes satellite-derived surface thermal patterns rather than direct human heat exposure, thermal comfort, or health outcomes; therefore, implications for public health and population-level heat risk remain indirect and require further assessment using population, meteorological, and health-related data.

Key points

- Nighttime land surface temperatures increased more consistently than daytime temperatures across Gujarat cities.
- Vegetation and built-up contrasts showed city-specific associations with urban thermal variability.
- RF–SHAP analysis identified distinct daytime and nighttime patterns of predictive attribution.

1. Introduction

The Surface Urban Heat Island (SUHI) effect is a well-established

* Corresponding author at: Environmental Engineering Department, L D College of Engineering, Ahmedabad, Gujarat, 380015, India.
E-mail address: ramiyagni91@gmail.com (Y. Rami).

https://doi.org/10.1016/j.scs.2026.108122
Received 1 August 2026; Received in revised form 3 November 2026; Accepted 13 November 2026
Available online 17 November 2026
2210-6707/© 2026 Elsevier Ltd. All rights are reserved, including those for text and data mining, AI training, and similar technologies.

urban climate phenomenon in which built environments exhibit higher surface temperatures than surrounding rural areas due to land cover change, altered surface energy balance, and anthropogenic heat emissions (Arnfield, 2003; Du et al., 2023; Oke, 1982; Santamouris et al., 2014). The replacement of natural surfaces by impervious materials reduces evapotranspiration, increases sensible heat flux, and enhances thermal storage, resulting in persistent surface and canopy-layer warming (Mathew et al., 2016). SUHI intensification can have important implications for public health, energy demand, air quality, and urban sustainability under accelerating climate change. Although satellite-derived surface thermal conditions can inform broader assessments of urban heat risk, their implications for human heat exposure and health depend on additional meteorological, demographic, and physiological factors that are not evaluated in this study (Chakraborty et al., 2022).

Recent global assessments further demonstrate that SUHI is characterized by substantial long-term and diurnal variability. Across 1,162 global cities, increasing trends in SUHI frequency and maximum duration have been observed during both daytime and nighttime, with background climate and surface properties showing strong associations with SUHI variability (Liu et al., 2025). Similarly, increasing spatial cohesion of SUHI has been reported across a majority of global cities, with vegetation and impervious-surface contrasts strongly influencing its spatial organization (Li & Gao, 2025).

In rapidly urbanizing countries such as India, urban thermal environments are evolving alongside extensive demographic growth, land-use change, and severe atmospheric pollution. Field and remote-sensing observations have documented pronounced urban heat-island effects in Indian cities, including strong thermal contrasts associated with densely built-up and commercial areas (Mohan et al., 2012). Consistent with recent global observations, numerous studies have documented pronounced SUHI effects across major Indian cities, although their magnitude and associated environmental characteristics vary considerably with climate, urban morphology, and land-cover characteristics (Mohan et al., 2011; Santamouris et al., 2015). Ahmedabad and Jaipur exhibit weak or inverse daytime SUHI but substantially stronger nighttime warming, highlighting pronounced diurnal asymmetry in urban thermal behaviour (Mathew et al., 2018; Nayak et al., 2023; Sultana & Satyanarayana, 2019). Studies in Kolkata, Nagpur, Guwahati, Chennai, and Delhi further demonstrate increasing urban temperatures associated with rapid urbanization, industrialization, vegetation loss, and expanding impervious surfaces (Mallick et al., 2013; Kotharkar & Bagade, 2018; Halder et al., 2021; Mohammad & Goswami, 2021). In the National Capital Region, long-term urban sprawl has also been linked to changes in urban heat-island intensity and thermal comfort (Mohan et al., 2020). Multi-city remote-sensing assessments consistently identify declining vegetation and increasing built-up intensity as important factors associated with urban thermal variability across Indian cities (Ghosh et al., 2022), while long-term satellite observations reveal that nighttime warming can exceed daytime warming, a pattern consistent with enhanced surface heat retention and reduced nocturnal cooling (Siddiqui et al., 2021). However, satellite-derived LST trends alone cannot directly quantify urban heat storage or establish the mechanisms responsible for nocturnal warming. More recent national-scale evidence further indicates that urbanization contributes substantially to the excess nighttime warming of Indian cities relative to surrounding non-urban regions (Sethi & Vinoj, 2024).

Given the difficulty of distinguishing the effects of multiple covarying factors on surface climate, recent studies have increasingly employed interpretable machine-learning approaches to examine nonlinear relationships and interactions associated with urban thermal variability (Chakraborty et al., 2021; Venter et al., 2021). Random Forest and gradient-boosting models combined with SHAP-based interpretation have demonstrated that vegetation, impervious surfaces, background climate, and urban characteristics exert heterogeneous influences on SUHI, with their relative importance differing between daytime and nighttime conditions (Fu et al., 2025; Ye et al., 2026).

In addition to land-cover transformation, aerosol loading may influence urban thermal conditions through radiative interactions and modifications of the surface energy balance (Li et al., 2011; Ramanathan et al., 2001). However, aerosol–UHI interactions are complex and may vary with regional climate, vegetation response, and time of day. Recent evidence indicates that aerosol reductions can modify urban–rural thermal contrasts indirectly through changes in solar radiation and vegetation dynamics, demonstrating that aerosol effects cannot be interpreted independently of land-surface processes (Zou et al., 2025). Urban thermal responses are also seasonally dependent, with stronger SUHI signatures commonly observed during pre-monsoon and winter periods under relatively dry and stable atmospheric conditions (Chakraborty et al., 2017).

Despite substantial advances in long-term and multi-city SUHI research, important questions remain regarding how changes in absolute land surface temperature (LST) relate to changes in urban–rural thermal contrasts, and how the relative importance of environmental predictors varies between daytime and nighttime conditions. Previous studies have characterized long-term SUHI variability across Indian cities (Ghosh et al., 2022; Nayak et al., 2023; Siddiqui et al., 2021) and examined urbanization-associated warming at the national scale (Sethi & Vinoj, 2024). However, further comparative analysis is needed to jointly examine diurnal LST and SUHI trends, urban–rural differences in vegetation, built-up intensity, aerosol loading and surface albedo, spatial thermal patterns, and city-specific environmental predictor attribution within a consistent regional framework.

To address this gap, this study investigates five major cities of Gujarat—Ahmedabad, Gandhinagar, Vadodara, Surat, and Rajkot—over 2000–2024 using an integrated satellite-based analytical framework. The study makes three principal contributions. First, it distinguishes long-term changes in absolute daytime and nighttime LST from changes in SUHI intensity, enabling an assessment of whether urban surface warming is accompanied by increasing urban–rural thermal contrasts. Second, it integrates urban–rural environmental contrasts, spatial thermal hotspot analysis, and Random Forest–SHAP attribution to examine the relative importance of vegetation, built-up intensity, aerosol loading, and surface albedo for the selection of cities. Third, it identifies city-specific and diurnal differences in the relative importance of these predictors, providing a comparative understanding of urban thermal variability across a common regional setting. By combining 25 years of daytime and nighttime observations with statistical trend analysis and interpretable machine learning, this study extends existing multi-city assessments by examining the relationships among thermal trends, environmental contrasts, spatial patterns, and model-attributed predictors within the rapidly urbanizing cities of western India.

2. Methodology

2.1. Study area

Gujarat, located in western India, experiences a hot semi-arid climate with summer temperatures frequently exceeding 45°C. Major heatwave events in 2010, 2016, and 2024 highlighted increasing urban heat vulnerability across the state (India Meteorological Department (IMD) 2026; Knowlton et al., 2014). Its extensive coastline (~1,600 km), rapid urbanization, industrial development, and contrasting coastal–inland climatic settings make Gujarat an important region for investigating SUHI dynamics in a semi-arid environment. Recent national-scale evidence further indicates substantial urbanization-linked nighttime warming across Indian cities, including rapidly developing cities in western India (Sethi & Vinoj, 2024).

2.1.1. Selection of cities and city characteristics

This study focuses on five Smart Cities of Gujarat—Ahmedabad, Gandhinagar, Vadodara, Surat, and Rajkot—selected to represent

diverse urban forms, climatic settings, vegetation conditions, population densities, industrial activities, and coastal influences (Government of India, 2015; Nayak et al., 2023). Together, these cities provide a comparative framework for assessing the spatial and temporal variability of SUHI across Gujarat (Fig. 1).

Ahmedabad, the largest city in Gujarat (~8.4 million population), is a dense inland metropolis characterized by a hot semi-arid climate, extensive impervious surfaces, rapid urban expansion, and limited green cover. Previous remote-sensing assessments have documented pronounced urban–rural thermal contrasts in Ahmedabad and linked its thermal environment to land-cover transformation and urban expansion (Mathew et al., 2018; Ghosh et al., 2022). The city experiences extreme summer conditions, with maximum temperatures often exceeding 46°C during the pre-monsoon season. The city has been widely recognized as a heat-risk hotspot and serves as an important benchmark for urban heat adaptation studies in India.

Gandhinagar, the state capital (~0.2 million population), represents a planned urban environment characterized by sector-based development, wide roads, and relatively high vegetation cover. Compared with other Gujarat cities, its lower density and greener urban morphology provide an opportunity to evaluate the influence of urban planning and vegetation on local thermal conditions and land surface temperature patterns.

Vadodara (~2 million population) is a rapidly growing city in central Gujarat characterized by mixed industrial, residential, and heritage land uses. Continued urban expansion and industrial development have altered surface characteristics and transformed the urban landscape, making it a valuable case for examining urban thermal variability

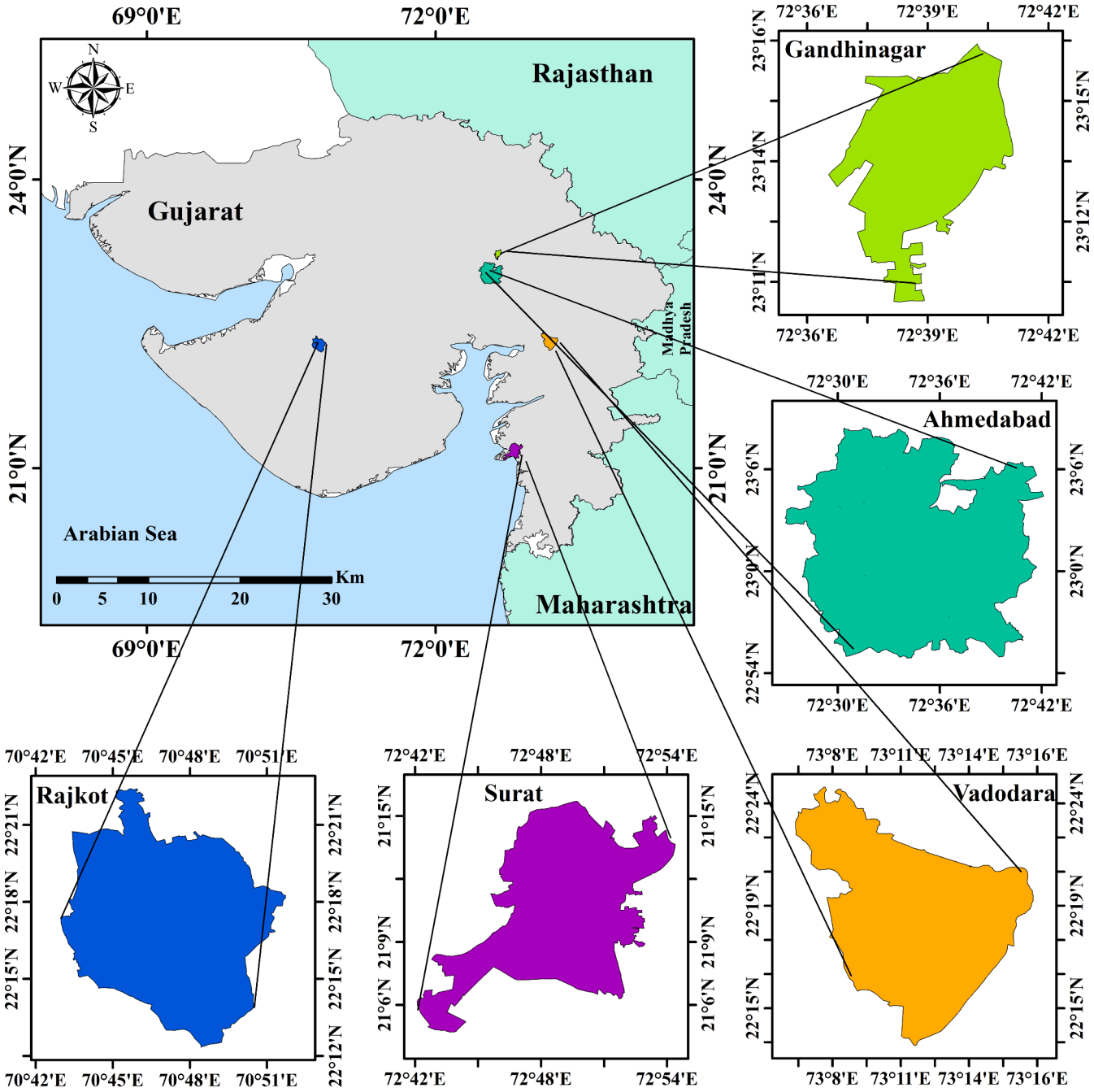

Fig. 1. Five smart cities of Gujarat State – Ahmedabad, Gandhinagar, Vadodara, Surat, and Rajkot.

associated with land-use change.

Surat (~7.5 million population) is a major coastal metropolis influenced by the Arabian Sea. High humidity, dense industrial development, extensive impervious surfaces, and limited green spaces shape the city's thermal environment despite maritime influences, providing insight into coastal controls on urban climate dynamics.

Rajkot (~2 million population) is a rapidly urbanizing inland city in the Saurashtra region characterized by a hot semi-arid climate, limited vegetation cover, and expanding built-up areas. Ongoing industrial growth and urban expansion have substantially modified land surface characteristics, particularly across newly developed urban areas during recent decades.

Together, the selected cities span gradients in climate, urban morphology, vegetation cover, industrialization, and coastal influence, while remaining within a common regional geographic setting. This configuration enables inter-city comparison of SUHI dynamics while reducing the large-scale climatic heterogeneity inherent in national or global multi-city assessments. The resulting framework provides an effective basis for evaluating city-specific thermal responses and their environmental controls across rapidly urbanizing western India.

2.2. Data sources and processing

2.2.1. Satellite and reanalysis datasets

This study employs multi-source satellite and meteorological datasets to quantify urban thermal dynamics, land-surface characteristics, atmospheric conditions, and urban environmental change across five major cities of Gujarat during 2000–2024 (Table 1). The combined use of satellite-derived LST with vegetation and built-up indicators has been widely applied for characterizing urban thermal dynamics and land-surface controls in Indian cities (Mathew et al., 2018; Ghosh et al., 2022; Siddiqui et al., 2021; Singh et al., 2022). MODIS-derived LST (Wan et al., 2021), NDVI, NDBI, AOD, and α were used to characterize urban thermal conditions, vegetation dynamics, built-up expansion, atmospheric loading, and surface reflectivity. Daytime and nighttime LST were analyzed to assess diurnal thermal behavior, NDVI served as a proxy for vegetation cover and evapotranspirative cooling, NDBI represented built-up intensity and impervious surface expansion, AOD characterized atmospheric aerosol loading, and albedo was used to evaluate changes in land-surface reflectivity.

The analysis was restricted to pixels within the municipal-boundary shapefiles of the five study cities or within the defined rural buffer zones, as applicable to each analysis. All datasets were processed using a common coordinate reference system. The 1-km LST coordinates served as the spatial reference, and the other satellite products were matched to these locations using the nearest available latitude–longitude coordinates after rounding coordinates to four decimal places. This procedure provided a common coordinate framework but did not harmonize the native spatial resolutions of the satellite products.

For the spatial comparison of long-term changes, ΔLST_t, $\Delta SUHI_t$, $\Delta NDVI_t$, $\Delta NDBI_t$, and ΔAOD_t were examined to assess their spatial associations across the five cities. Here, Δ_t denotes the temporal change between 2001 and 2024, calculated as the 2024 value minus the 2001 value. The change for each variable was defined as the difference between its 2024 and 2001 values (Δ_t). Because the input datasets differ in native spatial resolution and spatial coverage, the spatial matching procedure and the number of valid observations were considered when interpreting the results.

2.2.2. Surface Albedo estimation

α was estimated from MODIS MCD43A3 White-Sky Albedo (WSA) and Black-Sky Albedo (BSA) partitioned using the diffuse radiation fraction (K_d) derived from ERA5 reanalysis following the approach of Chakraborty et al. (2021):

$$\alpha = K_d \cdot \mathrm{WSA} + (1 - K_d) \cdot \mathrm{BSA}$$

The annual albedo values were subsequently used for temporal trend analysis and inter-city comparisons.The MCD43A3 product provides bidirectional reflectance distribution function (BRDF)-corrected white-sky and black-sky albedo estimates, which have been extensively validated for regional and global land surface studies (Lucht et al., 2000; Schaaf et al., 2002).

2.2.3. Data processing and aggregation

All datasets were processed using Google Earth Engine (GEE) and local post-processing workflows. GEE enables cloud-based processing of multi-temporal satellite datasets while preserving native spatial and temporal resolutions for large-scale environmental analyses (Gorelick et al., 2017). LST, NDVI, NDBI, and albedo were processed within GEE, whereas AOD data were downloaded and processed locally prior to annual aggregation. Standard quality-assurance (QA) filtering recommended for each MODIS product was applied to remove cloud-contaminated and low-quality observations prior to annual compositing (Didan, 2015; Vermote, 2015). MODIS products incorporate product-specific cloud screening and quality-assessment procedures and, where applicable, atmospheric correction. Nevertheless, residual cloud contamination and variations in valid observation availability may persist, potentially introducing temporal sampling bias. NDVI was obtained directly from MOD13A2, whereas NDBI was derived from MOD09A1 surface reflectance following the approach of Zha et al. (2003). Similar integration of remotely sensed LST, NDVI, and NDBI has been employed to characterize long-term urbanization and thermal variability in Indian cities (Ghosh et al., 2022; Singh et al., 2022).

For 2000–2024, annual and seasonal city-level estimates were derived from quality-filtered satellite observations using the median of available valid observations. Sen's slopes and Mann–Kendall trend statistics were calculated from the resulting annual city-level series; therefore, the reported slopes describe trends in annual median-based estimates rather than annual means or individual daily observations. For all variables, temporal inputs were based on the available satellite

Table 1
Satellite datasets used for urban climate analysis.

Variable	Product V6.1	Resolution		Derived Indicator	Purpose	Method / Key Notes	Reference
		Spatial	Temporal				
Land Surface Temperature	MOD11A2	1 km	8-day composite	Daytime and Nighttime LST	Surface thermal dynamics and SUHI assessment	QA-filtered observations	Wan (2021)
Vegetation Index	MOD13A2	1 km	16-day composite	NDVI	Vegetation cover and evapotranspiration proxy	Used to characterize vegetation dynamics	Didan (2021), Vermote (2015)
Built-up Index	MOD09A1	500 m	8-day composite	Derived from SWIR Band 6 and NIR Band 2	Urbanization intensity and impervious surfaces	NDBI= (SWIR−NIR)/ (SWIR+NIR)	Zha et al. (2003)
Aerosol Optical Depth	MOD04_3K	3 km	Daily (aggregated)	AOD	Atmospheric loading and aerosol–thermal interactions	City-scale annual aggregation	Levy et al. (2013)
Surface Albedo	MCD43A3	500 m	16-day composite	WSA, BSA, Albedo (α)	Surface reflectivity trends	$\alpha = K_d \times WSA + (1-K_d) \times BSA$ using ERA5 diffuse fraction	Chakraborty et al. (2021)

composite observations rather than raw daily measurements. Annual and seasonal statistics were calculated using the median of available valid observations. Summer was defined as February–May, monsoon as June–September, and winter as October–January. Spatial aggregation was performed at the city scale by extracting mean values over predefined urban extents. Missing observations associated with cloud cover or retrieval uncertainty were handled by excluding missing observations from statistical calculations; valid zero-valued entries were retained for derived variables. No additional minimum-observation threshold was imposed; therefore, annual and seasonal medians were calculated from the available valid observations for each period. Years with incomplete temporal coverage were retained when valid observations were available, and the number of contributing observations could consequently vary among years. To preserve the intrinsic spatial characteristics of each dataset, no spatial resampling or resolution homogenization was applied; all variables were analyzed at their native resolutions and subsequently aggregated for inter-city comparison. The same quality-filtering, missing-value treatment, and temporal aggregation procedures were applied to daytime and nighttime datasets. However, the number of valid observations contributing to individual estimates could vary with data availability. Seasonal estimates were not assigned equal weights through an additional averaging step; annual and seasonal medians were calculated using the same median-based logic. Although quality filtering was applied, uneven temporal coverage may still introduce sampling bias that cannot be fully excluded (Table S6 and S7). In addition, differences in native spatial resolution, residual retrieval errors, and variations in the number of valid observations may introduce uncertainty into annual and seasonal estimates. These uncertainties were not quantitatively propagated through the analysis and should be considered when interpreting the results.

2.2.4. Spatial framework

Urban boundaries for Ahmedabad, Gandhinagar, Rajkot, Surat, and Vadodara were delineated using administrative city limits. The latest available municipal boundaries were used as a fixed spatial framework for the entire 2000–2024 study period; the boundaries and corresponding rural reference zones were not updated annually. City-specific rural reference areas were defined as 5-km-wide annular zones: 25–30 km beyond the Ahmedabad municipal boundary, 2–7 km beyond the Gandhinagar, Rajkot, and Vadodara municipal boundaries, and 5–10 km beyond the Surat municipal boundary. These distances were selected considering the surrounding urban geography and land-use patterns to minimize the inclusion of neighbouring urban areas within the rural reference zones. In particular, the more distant reference zone for Ahmedabad was selected to avoid potential overlap with the neighbouring urban area of Gandhinagar. Urban–rural contrast frameworks are widely employed in satellite-based SUHI assessments because they explicitly quantify the thermal difference between built-up urban surfaces and their non-urban background (Mathew et al., 2018; Ghosh et al., 2022; Liu et al., 2025). This framework ensured consistent assessment of SUHI intensity and urban–rural environmental contrasts (ΔNDVI, ΔNDBI, ΔAOD, and ΔAlbedo). The same spatial framework was also used to evaluate both the city-level SUHI and its intra-urban variability, facilitating multi-scale assessment of urban climate change across the study cities.

Two structural constraints inherent to the spatial data processing should also be noted. The study utilized fixed municipal administrative boundaries delineated from the latest available years and kept constant across the entire 2000–2024 study period. Because these rapidly growing cities experienced massive outward sprawl over these two decades, static administrative masks introduce temporal non-stationarity. Land pixels classified as urban core in 2000 may have been peripheral or rural agricultural land at the beginning of the record, which can systematically bias long-term Sen's slope trend estimations. Additionally, the analysis deliberately preserved native sensor spatial resolutions without homogenization, combining datasets with different spatial supports, including 1-km LST and 3-km AOD products. Since a single 3-km AOD pixel encompasses an area nine times larger than a standard 1-km LST pixel, forcing these disparate spatial supports into a shared zonal grid introduces spatial smoothing errors, rendering coarse-scale aerosol comparisons less sensitive to localized urban microclimates.

2.3. Urban thermal assessment framework

This study adopts an integrated analytical framework to quantify multi-dimensional urban surface heating across five major urban agglomerates of Gujarat (Fig. 2). The framework follows widely adopted thermal remote sensing principles for integrating satellite-derived land surface temperature with environmental indicators to characterize urban thermal environments (Voogt & Oke, 2003; Weng, 2009). The methodology combines satellite-derived thermal and land-surface indicators to evaluate urban thermal conditions and their spatial variability. It does not directly assess human heat exposure, population vulnerability, or thermal comfort. Recent multi-city studies have similarly demonstrated the value of integrating long-term thermal observations with vegetation, impervious-surface, climatic, and other environmental indicators to resolve the interacting environmental associations with SUHI variability (Ghosh et al., 2022; Li & Gao, 2025; Liu et al., 2025). As illustrated in Fig. 2, the workflow includes data acquisition, preprocessing, derivation of thermal indicators (LST and SUHI), and environmental predictors (NDVI, NDBI, and AOD). These datasets were subsequently subjected to trend detection, change-point analysis, univariate and multivariate regression analyses, and machine-learning-based attribution to examine the environmental associations and relative predictive contributions to daytime and nighttime SUHI variability. Finally, spatial analyses were conducted to examine the long-term evolution of urban thermal patterns and environmental gradients across the five study cities.

The methodology integrates satellite-derived land surface temperature (LST) with land-surface and environmental indicators to characterize urban thermal patterns. Because the thermal analysis is based on satellite-derived LST, the study assesses surface urban heat island (SUHI) patterns and intra-urban surface thermal anomalies, rather than near-surface air-temperature UHI, canopy-layer UHI, or boundary-layer UHI. Human heat exposure and thermal comfort are not directly assessed.

2.3.1. Surface urban heat island (SUHI) assessment

SUHI intensity was quantified using two complementary approaches: Method 1, Regional SUHI Assessment (Urban–Rural Thermal Contrast), and Method 2, Local SUHI Assessment (Within-City Thermal Variability). This dual framework distinguishes city-scale urban–rural thermal amplification from localized intra-urban thermal heterogeneity, both of which are recognized as complementary dimensions of surface urban heat assessment (Voogt & Oke, 2003; Mathew et al., 2018; Ghosh et al., 2022).

2.3.1.1. Regional SUHI assessment (urban–rural thermal contrast). Urban boundaries were defined using municipal limits, while city-specific rural reference zones were delineated using buffer annuli extending outward from each urban boundary. The rural reference zones comprised the 25–30 km annulus for Ahmedabad, the 2–7 km annulus for Gandhinagar, Rajkot, and Vadodara, and the 5–10 km annulus for Surat. In each case, the inner buffer defines the excluded zone surrounding the urban boundary, while the area between the inner and outer buffers represents the rural reference zone (Figure S5). The selection of city-specific buffer distances was guided by Kumar et al. (2017), who used non-urban reference strips at distances that varied according to urban area size, and by visual inspection of the surrounding land-use patterns using Google Earth. This approach allowed the rural reference zones to be delineated in the context of the spatial characteristics of each city.

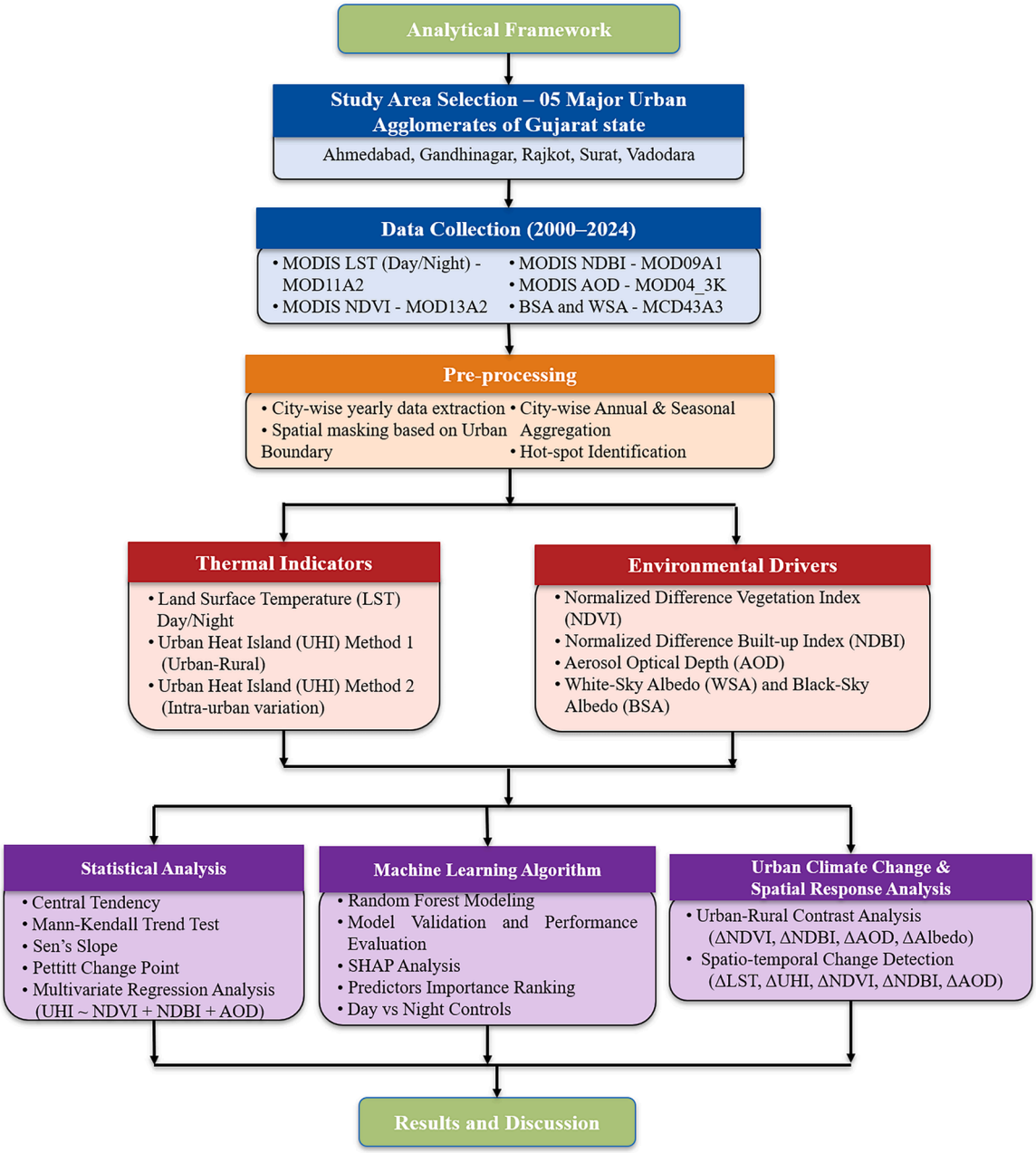

Fig. 2. Analytical framework for assessing spatiotemporal urban thermal dynamics and environmental drivers across major urban agglomerations of Gujarat (2000–2024).

Similar urban–rural thermal contrast approaches have been widely applied in MODIS-based and multi-city SUHI assessments to characterize city-scale thermal amplification (Kumar & Mishra, 2019; Mathew et al., 2018; Ghosh et al., 2022; Siddiqui et al., 2021). Mean LST values were extracted for urban and rural zones, and SUHI intensity was calculated as:

$$SUHI = LST_{urban} - LST_{rural}$$

where SUHI represents the surface urban heat island intensity (°C) of the entire city, LST_{urban} is the spatially averaged land surface temperature of the urban area (°C), and LST_{rural} is the spatially averaged land surface temperature of the rural reference buffer (°C). No DEM-based elevation correction or elevation-matching procedure was applied in this study. Accordingly, the calculated SUHI represents the observed urban–rural LST contrast, which may include potential contributions from elevation differences between the two zones. Because the buffer distances differ among cities, the resulting SUHI estimates are based on city-specific rural reference zones, which should be considered when interpreting differences in SUHI magnitude across cities. Uncertainty in urban and rural LST estimates may affect the calculated SUHI intensity. The selection of rural reference zones, municipal boundary delineation, and surrounding land-cover heterogeneity may also influence SUHI estimates and inter-city comparisons.

2.3.1.2. Local SUHI assessment (intra-urban thermal anomaly). We also characterized within-city surface thermal variability using the minimum valid LST observed within each city boundary on each individual date as the reference temperature. Unlike a persistent minimum derived across the study period, this daily reference is recalculated for each observation date, allowing pixel-level thermal conditions to be evaluated relative to the coolest observed urban surface on the same date. The reference may

represent relatively cool surfaces, including vegetation and water bodies, depending on their presence and the availability of valid LST observations (Mohan et al., 2012). As this method quantifies relative temperature differences within the urban boundary rather than the urban–rural temperature contrast, it is interpreted as an intra-urban surface thermal anomaly rather than conventional SUHI intensity. The anomaly for each pixel was calculated as:

$$SUHI_{i,d} = LST_{i,d} - LST_{min,d}$$

where $SUHI_{i,d}$ is the SUHI intensity at pixel i on date d (°C), $LST_{i,d}$= land surface temperature of pixel i on date d (°C), $LST_{min,d}$= Persistent minimum LST observed within the urban boundary on the same date (°C). The pixel-level estimates identify localized hotspots and characterize spatial thermal variability within urban areas. When combined with the urban–rural SUHI intensity calculated in the preceding section, this metric provides a complementary assessment of regional urban–rural thermal contrasts and intra-urban surface temperature differences. Previous studies have demonstrated the value of complementary intra-urban thermal metrics for identifying surface temperature hotspots without relying exclusively on an urban–rural reference (Martin et al., 2015), including approaches based on percentile-defined thermal thresholds (Shreevastava et al., 2019). For clarity, Method 1 was used as the SUHI metric for the Random Forest–SHAP analysis, whereas Method 2 was used for the city-wise bivariate regression analysis (Fig. 6) and the spatial temporal-change analysis (Fig. 9). Fig. 4 presents both formulations for comparison of their daytime and nighttime behaviour. Accordingly, the SUHI formulation is identified explicitly as Method 1 or Method 2 wherever the analytical metric differs.

To assess the robustness of trend significance, an autocorrelation-adjusted Mann–Kendall (MK) procedure was applied to account for potential serial dependence in the annual time series. The Benjamini–Hochberg (BH) procedure was then applied to the adjusted MK p-values across the 20 annual daytime and nighttime LST and SUHI trend series to obtain BH-adjusted q-values and account for multiple testing. The original MK results were retained for comparison with the adjusted results. Trend direction and magnitude were interpreted separately from statistical significance, and the adjusted p-values and BH-adjusted q-values were used to evaluate the robustness of the identified trends.

2.3.2. *Machine learning-based predictive attribution of surface urban heat island variability*

To examine the relative predictive contributions of environmental variables to surface urban heat island (SUHI) intensity, SHapley Additive exPlanations (SHAP) analysis was applied to Random Forest (RF) regression models (Breiman, 2001; Lundberg & Lee, 2017). Recent urban-heat studies have demonstrated the utility of tree-based machine-learning models coupled with SHAP interpretation for examining nonlinear relationships and the relative predictive contributions of environmental and urban-form characteristics to UHI/SUHI variability (Fu et al., 2025; Ye et al., 2026). Separate daytime and nighttime models were developed using annual observations from Ahmedabad, Gandhinagar, Rajkot, Surat, and Vadodara for 2000–2024. Each pooled dataset comprised 125 city-year observations (five cities × 25 years). Four urban–rural contrast variables were used as predictors: ΔNDVI, ΔNDBI, ΔAOD, and Δα (albedo contrast). These variables represent complementary land-surface and atmospheric characteristics potentially associated with SUHI variability, including vegetation conditions, built-up characteristics, aerosol–radiation interactions, and surface radiative properties (Li & Gao, 2025; Singh et al., 2022; Zou et al., 2025).

Because SUHI and the predictor variables were defined as urban–rural contrasts, their associations may partly reflect shared land-surface transformation processes. Potential predictor redundancy was assessed using pairwise Pearson correlation coefficients and variance inflation factors (VIFs). The strongest pairwise correlation was observed between ΔNDVI and ΔNDBI (r = −0.699), followed by ΔNDVI and ΔAOD (r = −0.486) and ΔNDBI and ΔAOD (r = 0.493). Correlations between ΔNDVI and Δα, ΔNDBI and Δα, and ΔAOD and Δα were −0.157, 0.457, and 0.392, respectively. The VIF values were 11.29 for ΔNDVI, 4.48 for ΔNDBI, 3.15 for ΔAOD, and 7.13 for Δα, based on 118 complete predictor records. These results indicate appreciable linear dependence among some predictors, particularly ΔNDVI and Δα. The correlation and VIF analyses were treated as exploratory diagnostics rather than definitive tests of RF model validity, because VIF assesses linear predictor dependence rather than the predictive validity of a Random Forest model. Furthermore, the pooled diagnostics may reflect both between-city differences and temporal variation; they do not establish the extent of predictor dependence within individual cities or across time. These limitations were considered when interpreting the SHAP attributions.

For pooled model-performance evaluation, separate daytime and nighttime datasets each comprised 125 observations (five cities × 25 years). Each dataset was divided into training and testing subsets using an 80:20 random split with random_state = 42, yielding 100 training observations and 25 testing observations per model. The RF regression models used 500 decision trees (n_estimators = 500) and a maximum tree depth of 4 (max_depth = 4). The remaining parameters were min_samples_split = 2, min_samples_leaf = 1, max_features = 1.0, and bootstrap = True; out-of-bag scoring was disabled (oob_score = False). Model performance was evaluated using the coefficient of determination (R^2), root mean square error (RMSE), and mean absolute error (MAE). No k-fold cross-validation, automated hyperparameter tuning, or out-of-bag performance evaluation was performed. Missing values in Δα were handled using median imputation, with medians estimated from the training data and applied to the corresponding test data. The same training-only imputation procedure was applied within the temporal and leave-one-city-out validation workflows. Because observations from the same cities and different years could be represented in both training and testing subsets, the random split assessed prediction for held-out observations from represented cities rather than generalization to future years or entirely unseen cities.

To examine temporal generalizability, the models were additionally trained using observations from 2000–2018 and evaluated on observations from 2019–2024. This temporal split comprised 95 training observations and 30 testing observations per diurnal model. To assess inter-city transferability, leave-one-city-out validation was performed by withholding all 25 annual observations from one city, training the model on the remaining four cities (100 observations), and predicting SUHI for the held-out city. This process was repeated for each of the five cities, and the predictions were pooled to calculate overall leave-one-city-out performance. R^2, RMSE, and MAE were calculated for both additional validation procedures. These validation strategies assessed different aspects of model performance: prediction for a later period and transferability to a city not represented in model training, respectively. Because the observations comprise repeated annual records from five cities, temporal dependence and persistent city-specific characteristics may also affect the apparent predictor–response relationships. The validation analyses were therefore used to assess temporal generalizability and inter-city transferability, while the limitations associated with pooled observations and shared environmental processes were considered when interpreting the results.

For the city-specific SHAP analysis, separate RF models were fitted for each city and diurnal period using all 25 annual observations available for that city. These models used 300 decision trees (n_estimators = 300), a maximum tree depth of 3 (max_depth = 3), and random_state = 42. For these city-specific models, missing values in Δα were handled by interpolation followed by backward and forward filling, as implemented in the analysis workflow. Because each city-specific model was fitted using all available observations for that city and was not independently evaluated on a held-out dataset, its SHAP results are interpreted as exploratory, model-dependent predictive

attributions rather than independently validated estimates of predictor effects.

To examine the direction and potential nonlinearity of predictor–response relationships, signed SHAP values were examined using SHAP dependence plots for ΔNDVI, ΔNDBI, ΔAOD, and Δα. These plots were generated separately for daytime and nighttime city-specific models to compare the relationships across Ahmedabad, Gandhinagar, Rajkot, Surat, and Vadodara (Supplementary Figures S2a and S2b). The nighttime ΔAOD dependence patterns were additionally presented to facilitate cross-city comparison (Supplementary Figure S3). Positive SHAP values indicate that a predictor's contribution shifts the model prediction above its expected output, whereas negative values indicate a shift below the expected output. These values describe model-based associations rather than causal effects.

First-order accumulated local effects (ALE) plots were also used to examine the overall shape of the fitted pooled-model responses to the four predictors under daytime and nighttime conditions (Supplementary Figure S4). ALE curves describe changes in model predictions over the observed predictor distributions and can help identify potential nonlinear response patterns. Both the dependence plots and ALE curves were interpreted cautiously because the dataset is limited in size, predictor dependence is present, and the city-specific models were not independently validated.

The RF model estimates SUHI intensity as a nonlinear function of the environmental variables:

$$\mathrm{SUHI} = f(\Delta\mathrm{NDVI}, \Delta\mathrm{NDBI}, \Delta\mathrm{AOD}, \Delta\alpha) \tag{1}$$

Correspondingly, the mean SHAP Importance is defined as:

$$I_j = \frac{1}{N}\sum_{i=1}^{N}\left|\phi_{ij}\right| \tag{2}$$

Where, I_j= importance of predictor j, N= total number of observations, ϕ_{ij}= SHAP value of predictor j for observation i.

Finally, the normalized SHAP Weight is given by:

$$W_j = \frac{I_j}{\sum_{j=1}^{m} I_j} \tag{3}$$

Where, W_j= normalized absolute SHAP importance of predictor j,m= total number of predictor variables. The normalized importance can be multiplied by 100 to express it as a percentage. For each city-specific model, the mean absolute SHAP value was calculated for each predictor and normalized by the sum of mean absolute SHAP values across all predictors. This yielded the normalized absolute SHAP attribution share (%) for ΔNDVI, ΔNDBI, ΔAOD, and Δα under daytime and nighttime conditions. These percentages represent each predictor's share of the total absolute SHAP attribution within the corresponding fitted model; they do not quantify the percentage of SUHI explained or caused by that predictor.

City-wise SHAP Contribution

$$C_{j,c} = \frac{\frac{1}{n_c}\sum_{i=1}^{n_c}\left|\phi_{ij,c}\right|}{\sum_{j=1}^{m}\left(\frac{1}{n_c}\sum_{i=1}^{n_c}\left|\phi_{ij,c}\right|\right)} \times 100 \tag{4}$$

Where, $C_{j,c}$= normalized absolute SHAP attribution share (%) of predictor $j$in city c, n_c= number of observations for city c, $\phi_{ij,c}$= SHAP value of variable $j$for observation $i$in city c. This framework enables the comparison of the relative predictive contributions of environmental variables to daytime and nighttime SUHI predictions. The normalized SHAP percentages represent relative predictor contributions within the fitted models; they do not represent percentages of SUHI caused by individual variables or independent causal effects. Potential correlations among the predictors may also affect their individual SHAP attributions.

Mean absolute SHAP values were used to summarize predictor importance, while signed SHAP values and dependence plots were used to examine the direction and potential nonlinearity of model-predicted relationships. Pooled ALE plots provided a complementary assessment of the fitted models' response patterns. Because the predictors may share correlated information and the city-specific models were fitted using only 25 annual observations without independent validation, these results are interpreted as exploratory, model-dependent associations rather than causal effects (Supplementary Figures S1–S4).

The analysis primarily uses satellite-derived surface variables and does not explicitly control for meteorological variability. Therefore, the estimated LST and SUHI trends represent observed surface-temperature changes and cannot be attributed exclusively to land-use or land-cover changes.

3. Results

3.1. Urban thermal intensification in Gujarat

Fig. 3 illustrates the interannual evolution of seasonal and annual daytime and nighttime LST across five major Gujarat cities during 2000–2024. Statistical trend metrics, including the Mann–Kendall test, Sen's slope, confidence intervals, Pettitt change-point analysis, and variance assessment, are summarized in Tables S1 and S2.

3.1.1. Daytime LST

Daytime LST exhibited pronounced seasonal variability across all cities, with summer temperatures ranging from 38–42°C, followed by monsoon (32–36°C) and winter (26–32°C) conditions (Fig. 3a–b). Ahmedabad, Rajkot, and Vadodara consistently recorded higher daytime temperatures than Gandhinagar and Surat, reflecting stronger inland surface heating and reduced maritime moderation, consistent with observations from Indian and global urban climate studies (Peng et al., 2012; Mathew et al., 2018; Ghosh et al., 2022; Mohammad & Goswami, 2021). Rajkot exhibited the largest seasonal thermal amplitude, whereas Surat showed comparatively moderated temperatures, likely due to coastal influences.

Annual daytime LST showed declining trends in all five cities, with Sen's slopes ranging from −0.066°C yr^{-1} in Surat to −0.145°C yr^{-1} in Rajkot (adjusted MK p = 0.0006–0.0721; BH-adjusted q = 0.0024–0.0962). Mean daytime LST ranged from 34.49°C in Surat to 36.81°C in Rajkot, indicating higher mean daytime surface temperatures in the inland cities than in Surat (Table S1). Rajkot exhibited the strongest declining trend ($\tau = -0.488$, $R^2 = 0.436$, adjusted MK p = 0.0006, BH-adjusted q = 0.0024), whereas Surat showed the weakest decline ($\tau = -0.357$, adjusted MK p = 0.0125, BH-adjusted q = 0.0192; Table S2). Despite interannual variability, these results indicate declining daytime surface temperatures rather than uniform daytime LST warming across the study cities. After BH correction, significant decreasing trends remained in Ahmedabad, Rajkot, Surat, and Vadodara ($q < 0.05$), whereas the decline in Gandhinagar was not statistically significant (q = 0.0962).

3.1.2. Nighttime LST

In contrast, nighttime LST exhibited a stronger and more persistent warming signal across the cities during 2000–2024 (Fig. 3). Summer nighttime temperatures generally ranged between 22–27°C, while winter temperatures varied between 15–21°C. Surat, Vadodara, and Ahmedabad exhibited the strongest nighttime warming trends, whereas Gandhinagar showed a comparatively weak and statistically non-significant trend.

Nighttime LST increased in all five cities, with Sen's slopes ranging from 0.049°C yr^{-1} in Gandhinagar to 0.108°C yr^{-1} in Surat. Mean nighttime LST ranged from 22.58°C in Rajkot to 24.04°C in Surat (Table S1). The strongest increasing trends occurred in Surat (0.108°C yr^{-1}; $\tau = 0.760$; $R^2 = 0.799$; adjusted MK $p = 4.02 \times 10^{-7}$; BH-adjusted $q = 8.0 \times 10^{-6}$), Vadodara (0.106°C yr^{-1}; $\tau = 0.569$; adjusted MK

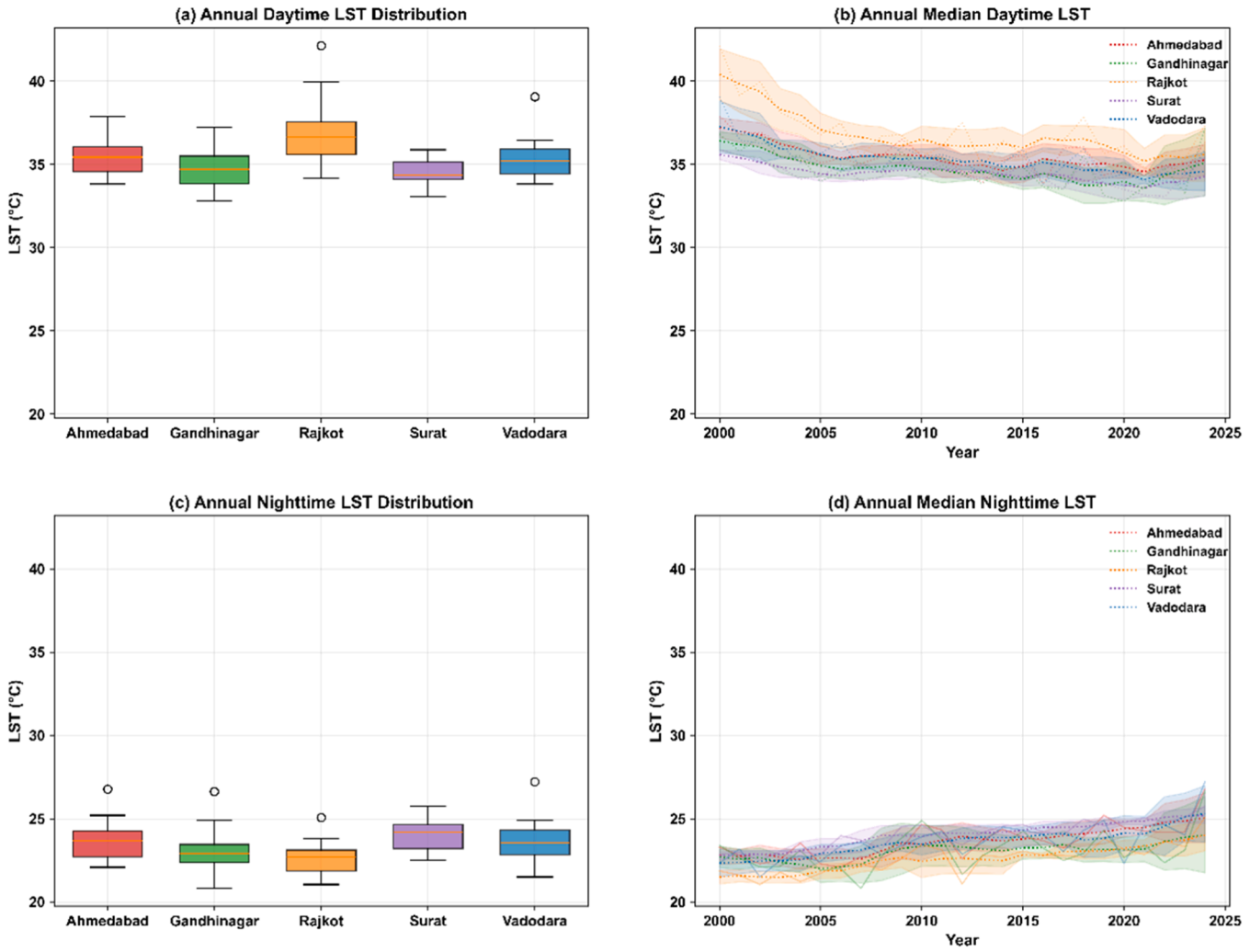

Fig. 3. Annual variability and interannual evolution of daytime and nighttime Land Surface Temperature (LST) across major cities of Gujarat during 2000–2024. *Panels (a) and (c) show the distributions of annual daytime and nighttime LST, respectively, using boxplots. Panels (b) and (d) show annual LST trajectories and centred five-year rolling means for daytime and nighttime conditions, respectively. Shaded bands represent ±1 rolling standard deviation (SD) around the five-year rolling mean, indicating local interannual variability rather than confidence intervals or uncertainty in the estimated mean. The rolling calculations use available observations at the series boundaries, where fewer than five years may contribute to the estimates.*

$p = 6.51 \times 10^{-5}$; BH-adjusted q = 0.000396), and Ahmedabad (0.096°C yr^{-1}; $\tau = 0.504$; adjusted MK p = 0.0026; BH-adjusted q = 0.0058). Rajkot also exhibited a significant increasing trend (0.090°C yr^{-1}; $\tau = 0.624$; adjusted MK $p = 3.36 \times 10^{-6}$; BH-adjusted $q = 3.4 \times 10^{-5}$), whereas the trend in Gandhinagar remained statistically nonsignificant after adjustment (adjusted MK p = 0.1682; BH-adjusted q = 0.2103; Table S2). The annual nighttime LST increased from 23.29 to 26.78°C in Ahmedabad, 23.39 to 26.63°C in Gandhinagar, 21.86 to 25.07°C in Rajkot, 22.84 to 25.74°C in Surat, and 22.33 to 27.22°C in Vadodara between 2000 and 2024. These endpoint values represent the observed annual estimates, whereas Sen's slope estimates the monotonic trend across the full annual series.

Overall, nighttime LST increased more consistently than daytime temperatures across the cities. The contrast between declining daytime LST and increasing nighttime LST indicates a pronounced diurnal asymmetry in surface-temperature trends. The physical mechanisms underlying this contrast and comparisons with previous studies are discussed in Section 4.0.

3.2. Temporal dynamics of surface urban heat island intensity

To assess temporal changes in urban–rural thermal contrasts, Surface Urban Heat Island (SUHI) intensity was evaluated using Method 1 (Urban–Rural Thermal Contrast). Fig. 4 presents the seasonal and annual evolution of daytime and nighttime SUHI during 2000–2024, while detailed statistics are summarized in Tables S1 and S2.

(a) Nighttime Urban Heat Island

Nighttime SUHI intensity differed substantially among cities during 2000–2024 (Figs. 4a–b and 5a). Vadodara and Surat exhibited the strongest nocturnal SUHI intensities, frequently exceeding 2.0–2.5°C after 2015 and generally ranging between 2.0 and 2.6°C, whereas Gandhinagar maintained comparatively weak thermal contrasts of approximately 1.0–1.7°C. Ahmedabad showed nighttime SUHI values typically ranging between 1.8 and 2.4°C, while Rajkot exhibited the weakest nocturnal signal (0.5–0.9°C).

Annual mean nighttime SUHI was 2.30 ± 0.23°C in Surat and 2.25 ± 0.24°C in Vadodara, compared with 2.04 ± 0.16°C in Ahmedabad, 1.47 ± 0.19°C in Gandhinagar, and 0.62 ± 0.14°C in Rajkot (Table S1). Trend analysis showed that nighttime SUHI increased significantly only in Vadodara (Sen's slope = +0.012°C yr^{-1}, p = 0.036). The trends were not statistically significant in Ahmedabad (+0.002°C yr^{-1}, p = 0.640), Gandhinagar (−0.003°C yr^{-1}, p = 0.607), Rajkot (−0.006°C yr^{-1},

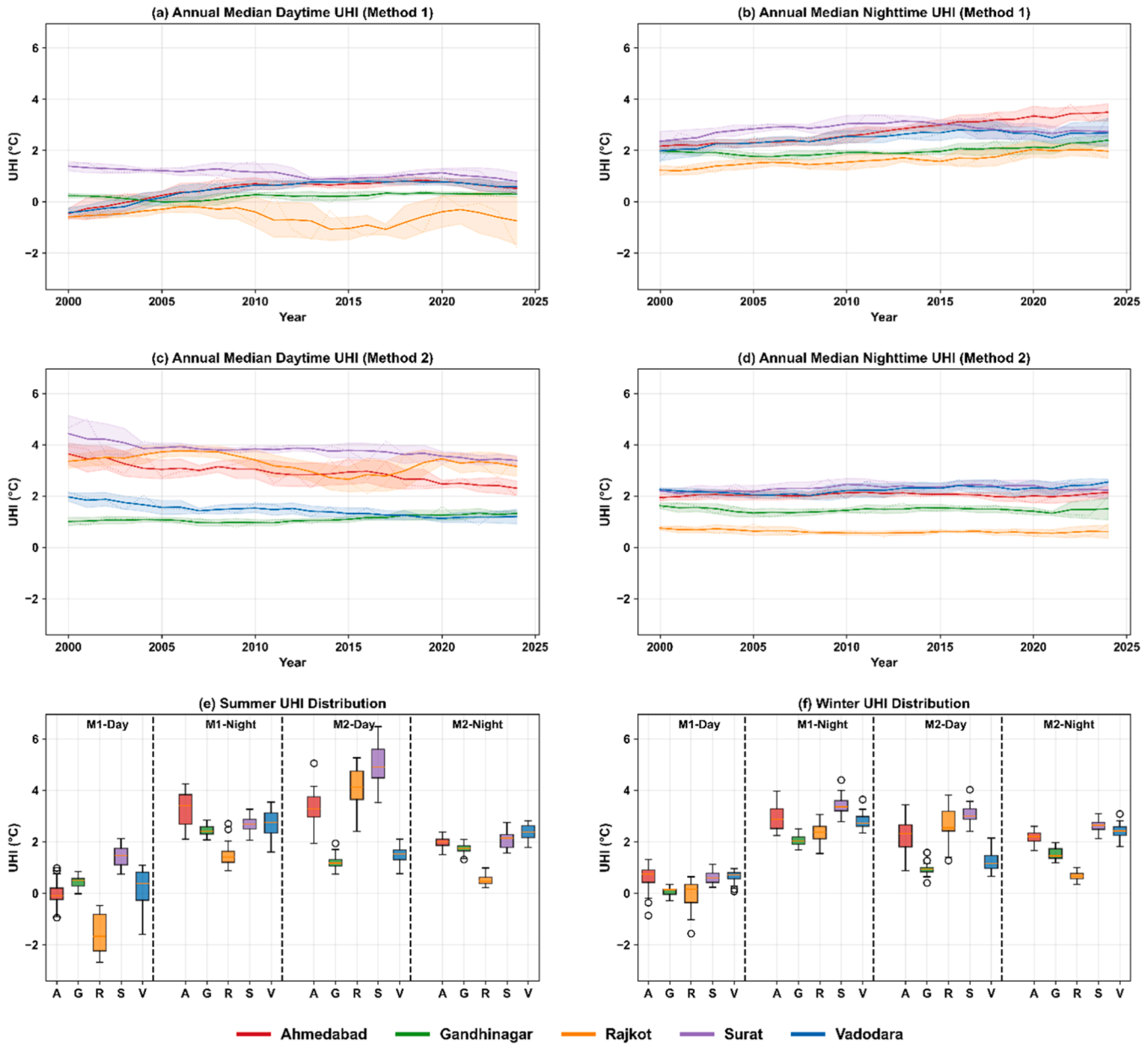

Fig. 4. ***Annual variability and interannual evolution of daytime and nighttime Surface Urban Heat Island (SUHI) intensity across major cities of Gujarat during 2000–2024****. Panels (a) and (b) show daytime and nighttime SUHI trajectories, respectively, using Method 1 (urban–rural thermal contrast), while panels (c) and (d) show the corresponding trajectories using Method 2 (intra-urban thermal contrast). Dotted lines represent annual values, solid lines indicate centred five-year rolling means, and shaded bands represent ±1 rolling standard deviation (SD), indicating local interannual variability rather than confidence intervals. Panels (e) and (f) show the summer and winter SUHI distributions, respectively, for both methods under daytime and nighttime conditions. Colours distinguish the five cities: Ahmedabad (red), Gandhinagar (green), Rajkot (orange), Surat (purple), and Vadodara (blue).*

$p = 0.176$), or Surat (+0.006°C yr^{-1}, $p = 0.362$) (Table S2). Thus, although nighttime SUHI was relatively high in Surat and Vadodara, a statistically significant long-term increase was detected only in Vadodara. Pettitt analysis identified a significant change point in nighttime SUHI for Vadodara in 2011 ($p = 0.032$); change points in the other four cities were not statistically significant ($p > 0.05$). Seasonal patterns further revealed differences in nighttime SUHI distributions, with generally stronger contrasts during summer and winter than during the monsoon season (Fig. 4).

(b) Daytime Urban Heat Island

Daytime SUHI exhibited greater temporal variability among cities and weaker or declining long-term trends in most cities (Figs. 4c–d and 5b). Surat and Rajkot consistently recorded the highest daytime SUHI magnitudes, frequently exceeding 2.5–3.0°C during summer and reaching 3.5–4.5°C during peak warming periods. Ahmedabad maintained elevated thermal contrasts of approximately 2.5–3.5°C, whereas Gandhinagar and Vadodara generally exhibited lower daytime SUHI intensities (<2°C and typically 1.0–1.8°C).

Mean daytime SUHI ranged from 1.11°C in Gandhinagar to 3.80°C in Surat, while Rajkot exhibited the greatest daytime variability (CV = 14.68%) among the inland cities (Table S1). The daytime SUHI trends differed by city. Ahmedabad showed a significant decrease (Sen's slope = −0.048°C yr^{-1}, $p < 0.001$), as did Surat (−0.030°C yr^{-1}, $p < 0.001$) and Vadodara (−0.030°C yr^{-1}, $p < 0.001$). Gandhinagar showed a significant increase (+0.013°C yr^{-1}, $p = 0.002$), whereas Rajkot exhibited a weak, statistically non-significant decrease (−0.022°C yr^{-1},

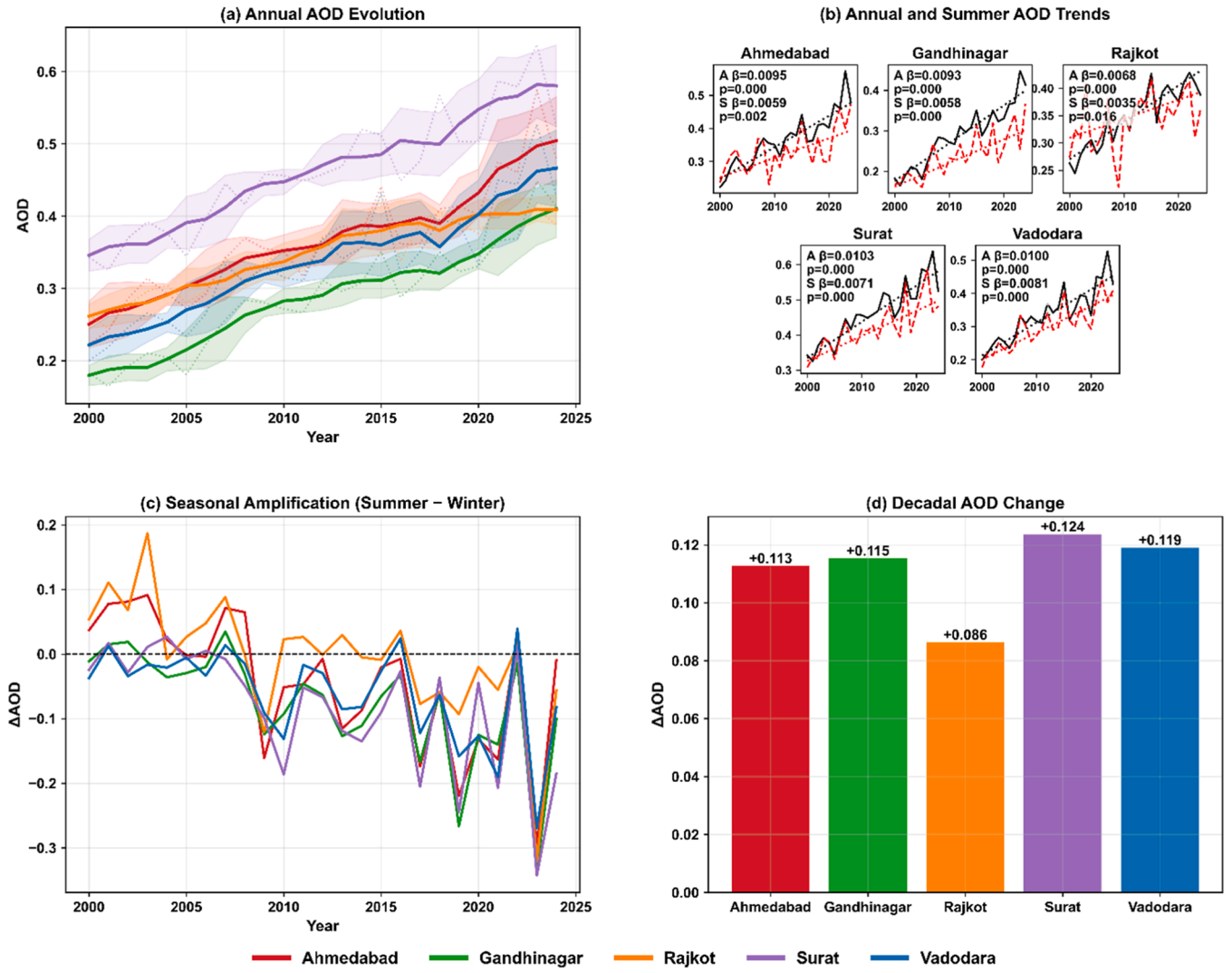

Fig. 5. Long-term evolution, trend diagnostics, seasonal amplification, and decadal change in AOD across major cities of Gujarat during 2000–2024. *Panel (a) presents annual AOD trajectories with 5-year rolling mean uncertainty bands. Panel (b) shows city-specific annual and summer AOD trends together with Sen's slope estimates (β) and Mann–Kendall significance levels (p). Panel (c) illustrates seasonal amplification expressed as the difference between summer and winter AOD. Panel (d) presents decadal changes in annual mean AOD between 2011–2024 and 2000–2010.*

p = 0.084) (Table S2). Summer consistently recorded the highest daytime SUHI intensities, whereas monsoon conditions exhibited lower thermal contrasts. These results indicate that daytime SUHI did not follow a uniform long-term trend across the five cities.

The LST trends provide additional context but should be distinguished from the SUHI trends. Nighttime LST increased significantly in Ahmedabad (+0.096°C yr^{-1}, adjusted MK p = 0.0026), Rajkot (+0.090°C yr^{-1}, p < 0.001), Surat (+0.108°C yr^{-1}, p < 0.001), and Vadodara (+0.106°C yr^{-1}, p < 0.001), whereas the positive trend in Gandhinagar (+0.049°C yr^{-1}) was not statistically significant (adjusted MK p = 0.1682). In contrast, daytime LST decreased significantly in four cities, with Sen's slopes ranging from −0.066°C yr^{-1} in Surat to −0.145°C yr^{-1} in Rajkot (Table S2), whereas Gandhinagar exhibited a different trend. These LST trends do not necessarily imply equivalent changes in urban–rural thermal contrasts.

The robustness of the identified SUHI trends was further assessed using autocorrelation-adjusted Mann–Kendall (MK) tests and Benjamini–Hochberg (BH)-adjusted q-values to account for multiple testing. Trend direction and magnitude were distinguished from statistical significance because adjustment may change the significance classification of individual city trends. Accordingly, the daytime SUHI decreases in Ahmedabad, Surat, and Vadodara and the increase in Gandhinagar should be interpreted in conjunction with their adjusted p-values and q-values. Similarly, the statistical significance of nighttime SUHI intensification in Vadodara should be assessed using the adjusted results rather than conventional MK p-values alone.

3.2.1. *Seasonal distribution and variability of SUHI intensity*

Fig. 4 summarizes the seasonal distribution and variability of SUHI intensity across Gujarat cities during 2000–2024. Daytime SUHI exhibited substantially greater intercity variability than nighttime conditions. Surat consistently recorded the highest daytime SUHI intensities, with median summer values approaching 5°C, followed by Rajkot (~4°C) and Ahmedabad (~3.3°C). In contrast, Gandhinagar and Vadodara maintained comparatively lower daytime SUHI magnitudes (<1.5°C). These observations are consistent with the annual statistics, where Surat recorded the highest mean daytime SUHI (3.80 ± 0.40°C) followed by Rajkot (3.30 ± 0.48°C) (Table S1). The wider interquartile ranges and extended whiskers observed in Surat and Rajkot indicate greater variability in their daytime SUHI distributions.

Nighttime SUHI distributions were comparatively more compact and stable across cities. Surat and Vadodara exhibited the highest nighttime median intensities (~2.4–2.7°C), followed by Ahmedabad (~2.2°C), whereas Rajkot consistently recorded the weakest nocturnal SUHI

(~0.5–0.6°C). Annual mean nighttime SUHI reached 2.30 ± 0.23°C in Surat and 2.25 ± 0.24°C in Vadodara, whereas Rajkot remained substantially lower (0.62 ± 0.14°C) (Table S1). The coefficients of variation, however, show that relative variability was highest in Rajkot at night (22.05%), followed by Gandhinagar (12.66%), Vadodara (10.48%), Surat (9.83%), and Ahmedabad (7.96%) (Table S1). Therefore, narrower absolute distributions should not be interpreted as uniformly lower relative variability across cities. Taken together, the seasonal distributions, descriptive statistics, and trend analysis distinguish the cities with high average SUHI intensity from those exhibiting statistically significant long-term changes.

3.3. Aerosol burden dynamics

3.3.1. Long-term changes in AOD

AOD was analyzed to assess long-term changes in atmospheric loading across Gujarat cities during 2000–2024. Fig. 5 illustrates the interannual evolution of annual and seasonal AOD, while detailed trend statistics are summarized in Tables S1 and S2. The annual AOD trajectories exhibit persistent upward trends across all cities, indicating sustained increases in aerosol burden over the study period, consistent with reported increases in anthropogenic emissions and aerosol loading across rapidly urbanizing regions of India (Dey & Di Girolamo, 2011; Ramachandran et al., 2012). Recent evidence further suggests that aerosol variability can influence urban–rural thermal contrasts through modifications of surface radiation and vegetation responses, although these effects remain secondary to land-cover transformation in most urban environments (Zou et al., 2025).

Surat and Vadodara recorded the strongest increases, with annual Sen's slopes approaching 0.01 yr^{-1}, whereas Rajkot exhibited the weakest but still positive trend (~0.007 yr^{-1}). The individual city-level trajectories further show Surat consistently occupying the upper concentration envelope, while Rajkot remained comparatively lower throughout the record.

Seasonal trends reveal increasing aerosol loading across all cities, particularly during summer conditions. However, seasonal amplification analysis (Summer − Winter) indicates a gradual shift from predominantly positive values during the early 2000s toward increasingly negative values after approximately 2010–2015 (Fig. 5). This transition suggests a relative strengthening of winter aerosol accumulation compared with summer conditions during the latter half of the study period. The strongest negative anomalies occurred during 2019–2023, particularly in Surat and Rajkot, indicating enhanced wintertime aerosol persistence. Comparable seasonal shifts toward enhanced winter aerosol accumulation have been attributed to reduced boundary-layer height, weaker atmospheric ventilation, and increased anthropogenic emissions during winter over the Indo-Gangetic Plain and western India (Dey & Di Girolamo, 2011; Ramachandran et al., 2012).

Decadal comparisons further confirm substantial increases in aerosol loading during 2011–2024 relative to 2000–2010 across all cities (Fig. 5). Surat and Vadodara exhibited the largest increases (~0.12), followed by Ahmedabad and Gandhinagar (~0.11), whereas Rajkot recorded the smallest but still substantial increase (~0.09). These results indicate that aerosol loading intensified markedly during the second half of the study period, particularly within industrialized and rapidly urbanizing urban centers. Similar long-term increases in aerosol loading have been reported for several rapidly expanding Indian metropolitan regions (Guha et al., 2018; Mohammad & Goswami, 2021). Nevertheless, recent national-scale analyses indicate that urbanization-related land-surface transformation is strongly associated with long-term urban warming, whereas aerosol-related influences appear secondary and regionally variable (Sethi & Vinoj, 2024).

Although vegetation and built-up contrasts showed stronger associations with urban thermal variability in most cities, aerosol loading contributed more substantially to model-predicted thermal variability in Rajkot and Surat. Recent studies indicate that aerosol effects on SUHI are complex because changes in aerosol loading can modify incoming solar radiation, vegetation productivity, and the urban surface energy balance (Chakraborty et al., 2021; Zou et al., 2025). Aerosol–thermal relationships have also been reported in Indian cities, while previous studies have highlighted the importance of land-cover transformation in urban warming (Chakraborty & Lee, 2019; Chakraborty et al., 2020; Guha et al., 2018; Mohammad & Goswami, 2021; Sethi & Vinoj, 2024). However, the present analysis does not isolate the independent causal effects of aerosols or land-cover changes from those of other correlated environmental variables.

Relationships Between SUHI and Environmental Predictors

To examine statistical relationships between SUHI intensity and selected environmental predictors, city-wise associations with NDBI, NDVI, and AOD were evaluated during 2000–2024 (Fig. 6). Detailed regression statistics are provided in Tables S1 and S2.

For daytime conditions (Fig. 6), NDBI showed positive associations in Ahmedabad and Rajkot, whereas negative associations were observed in Gandhinagar, Surat, and Vadodara; the strongest relationship was observed in Vadodara ($R^2 = 0.54$), despite its negative slope, followed by Ahmedabad ($R^2 = 0.34$). NDVI showed positive associations in Ahmedabad, Rajkot, and Surat, while negative associations were observed in Gandhinagar and Vadodara, with the strongest positive regression slope in Ahmedabad ($\beta = 16.59$). These city-specific built-up and vegetation associations are consistent with previous multi-city evidence linking impervious-surface intensity and vegetation characteristics to urban heat (Chakraborty et al, 2019). AOD showed negative associations in Ahmedabad, Rajkot, Surat, and Vadodara, while a positive association was observed in Gandhinagar ($R^2 = 0.30$). These results indicate that built-up intensity, vegetation, and aerosol loading were statistically associated with daytime SUHI variability, although the strength of these relationships differed among cities. Similar associations between land-cover characteristics and SUHI have been reported in previous studies (Chakraborty & Lee, 2019; Sethi & Vinoj, 2024). The individual regressions, however, do not establish independent causal effects.

These results suggest that the individual predictors captured less of the variation in nighttime SUHI than in daytime SUHI. Nocturnal thermal variability may be associated with differences in surface heat retention, atmospheric mixing, and nocturnal cooling. However, these processes were not directly measured, and their individual contributions to nighttime SUHI variability were not quantified in this analysis.

Overall, the regression results indicate differences in the strength of environmental associations between daytime and nighttime SUHI and among the five cities. Previous studies have also identified relationships between land-cover transformation and SUHI variability, while highlighting the complexity of urban thermal patterns (Chakraborty et al., 2020; Du et al., 2023). The present regression analysis identifies statistical associations rather than independently establishing the causal effects of vegetation loss, built-up expansion, or aerosol loading.

3.4. Urban–rural environmental contrast and thermal intensification

Urban–rural environmental contrasts were assessed using ΔNDVI, ΔNDBI, ΔAOD, and ΔAlbedo, representing differences in vegetation cover, built-up intensity, aerosol loading, and surface reflectivity between urban and surrounding rural areas (Fig. 7). These indicators characterize spatial differences in environmental conditions that may be associated with SUHI variability.

ΔNDVI values were consistently negative across all cities, indicating lower vegetation indices in urban areas than in the surrounding rural landscapes. Surat exhibited the largest vegetation contrast (ΔNDVI = −0.171), followed by Ahmedabad (−0.162), Vadodara (−0.134), Rajkot (−0.100), and Gandhinagar (−0.079). The larger-magnitude negative values in Surat and Ahmedabad indicate more pronounced urban–rural vegetation deficits. Such differences may be relevant to variations in evapotranspiration and surface temperature,

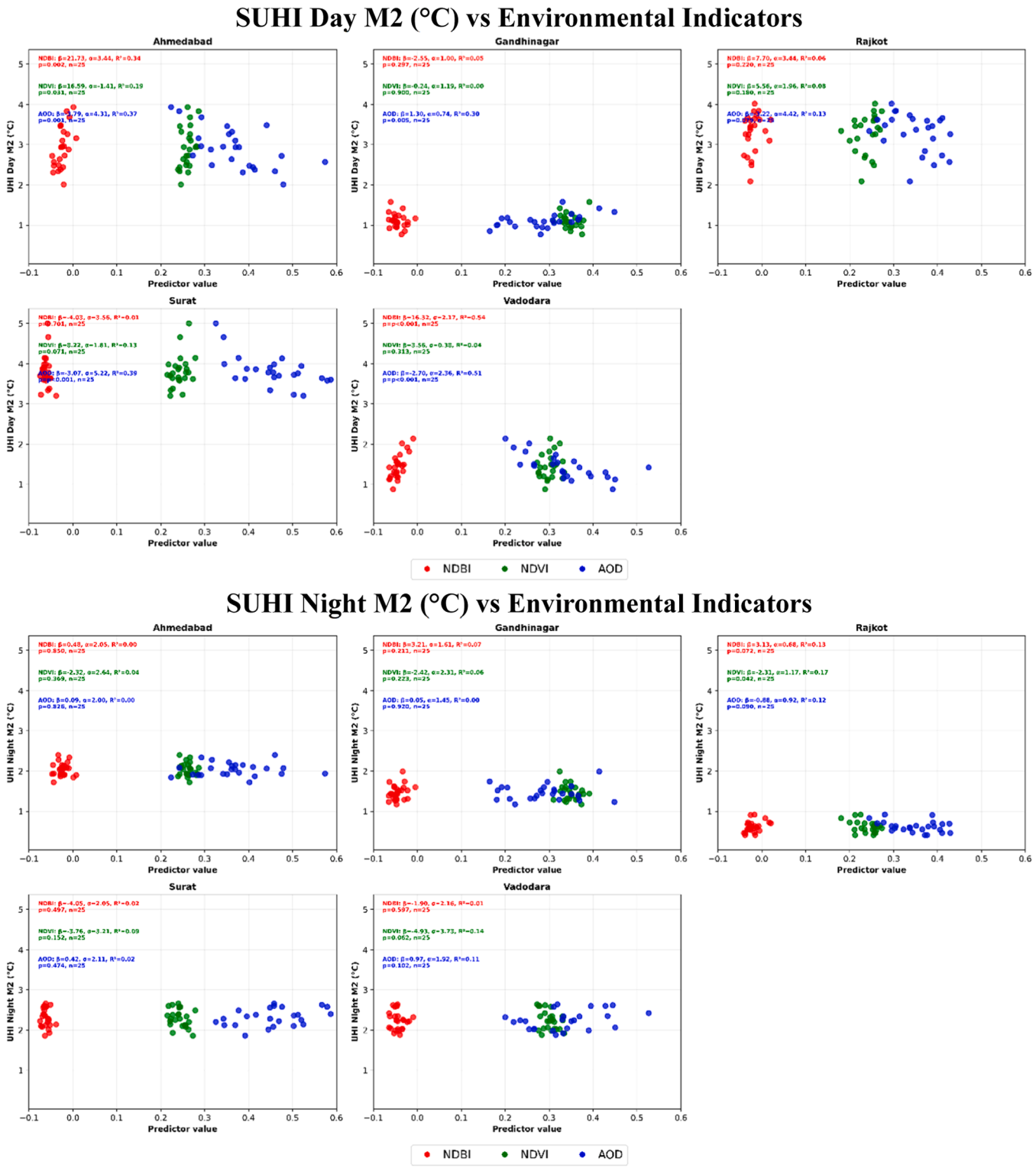

Fig. 6. City-wise relationships of daytime and nighttime SUHI intensity with built-up expansion, vegetation dynamics, and aerosol loading. ***Each predictor was evaluated using a separate univariate ordinary least-squares linear regression for each city and diurnal period. The reported statistics include the regression slope (β), intercept (α), coefficient of determination (R^2), p-value, and sample size (n). These regressions represent individual bivariate associations rather than a joint multivariable model. Differences in predictor scales and physical meanings should be considered when comparing slopes. The results indicate associations and should not be interpreted as causal effects.***

although the contrasts alone do not quantify changes in cooling or establish a causal effect on SUHI. Comparable relationships between vegetation indices and urban thermal conditions have been reported across Indian cities (Ghosh et al., 2022; Singh et al., 2022). The broader association between urban vegetation and thermal environments is also documented in previous research (Bowler et al., 2010; Chakraborty & Lee, 2019; Cuthbert et al., 2022; Li et al., 2011).

ΔNDBI values were predominantly positive and generally increased

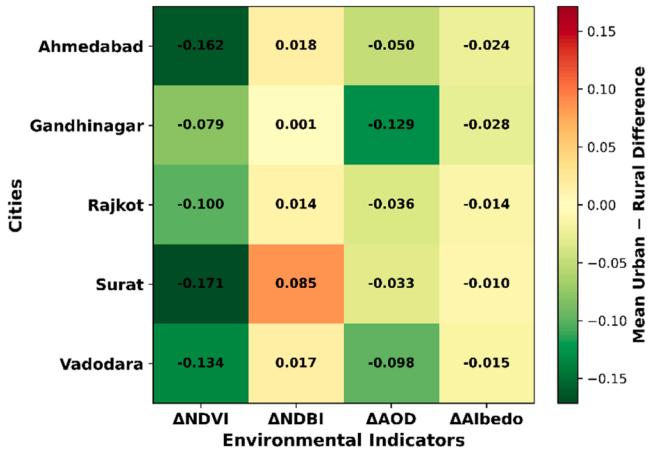

Fig. 7. Urban–Rural Environmental Differences Across Major Gujarat Cities During 2000–2024. All variables are unitless.

over time, indicating stronger built-up intensity in urban areas relative to their rural surroundings. Surat recorded the highest built-up contrast (ΔNDBI = 0.085), followed by Ahmedabad (0.018), Vadodara (0.017), Rajkot (0.014), and Gandhinagar (0.001). These results indicate substantial differences among cities in the magnitude of their urban–rural built-up contrasts. Previous studies have associated urban densification and impervious surfaces with elevated land surface temperatures (Guha et al., 2018; Sethi & Vinoj, 2024; Weng et al., 2004; Zhao et al., 2014). Positive relationships between NDBI and LST have also been reported in Indian remote-sensing studies (Ghosh et al., 2022; Singh et al., 2022). However, the present contrasts do not independently quantify the effects of built-up characteristics on SUHI or establish that changes in impervious surfaces caused the observed thermal patterns.

ΔAOD exhibited negative values across all five cities, indicating lower AOD in the urban areas than in their surrounding rural areas under the adopted urban–rural differencing convention. Gandhinagar exhibited the largest-magnitude aerosol contrast (ΔAOD = −0.129), followed by Vadodara (−0.098), Ahmedabad (−0.050), Rajkot (−0.036), and Surat (−0.033). ΔAlbedo was also negative across all cities, indicating lower urban surface reflectivity relative to surrounding rural areas. Gandhinagar (ΔAlbedo = −0.028) and Ahmedabad (−0.024) exhibited the largest-magnitude albedo contrasts, followed by Vadodara (−0.015), Rajkot (−0.014), and Surat (−0.010). Aerosols and surface albedo can influence urban thermal conditions through radiative and surface-energy-balance processes (Chakraborty & Lee, 2019; Du et al., 2023; Jin et al., 2005; Ramanathan et al., 2001). However, the magnitude of an urban–rural contrast alone does not establish the strength or direction of its independent association with SUHI. Recent research also highlights the complexity and spatial heterogeneity of aerosol–thermal relationships and their interactions with incoming solar radiation and vegetation dynamics (Zou et al., 2025).

The heatmap summary (Fig. 7) revealed negative ΔNDVI and ΔAlbedo values and positive ΔNDBI values across all five cities. Surat exhibited the largest-magnitude vegetation contrast (ΔNDVI = −0.171) and the highest built-up contrast (ΔNDBI = 0.085). Ahmedabad also showed a substantial vegetation contrast (ΔNDVI = −0.162) but a smaller built-up contrast (ΔNDBI = 0.018). Gandhinagar exhibited the smallest built-up contrast (ΔNDBI = 0.001) and the largest-magnitude aerosol contrast (ΔAOD = −0.129). These patterns demonstrate substantial inter-city differences in environmental conditions. They are broadly consistent with previous multi-city studies examining relationships between land-cover transformation and SUHI variability (Chakraborty et al., 2020; Fu et al., 2025; Ghosh et al., 2022; Sethi & Vinoj, 2024). Nevertheless, the descriptive contrasts and heatmap do not quantify the independent contributions of individual environmental variables to SUHI. Their relative predictive contributions are examined separately through the regression and RF–SHAP analyses.

3.5. Machine learning-based attribution of urban heat island variability

3.5.1. Development and performance of random forest models

To investigate the combined and potentially nonlinear relationships between urban–rural environmental differences and surface urban heat island (SUHI) intensity, Random Forest (RF) models were developed separately for daytime and nighttime conditions using ΔNDVI, ΔNDBI, ΔAOD, and ΔAlbedo as predictor variables. Model performance was first evaluated using a random 80:20 training–testing split, followed by temporal and leave-one-city-out validation to assess predictive performance under more stringent testing conditions. Each diurnal dataset comprised 125 observations (five cities × 25 years), corresponding to 100 training and 25 testing observations under the random split. Because observations from all five cities and multiple years were represented in the training dataset, this split evaluated predictions for held-out observations from cities already represented during training rather than generalization to entirely unseen cities or future periods.

The daytime model achieved an R^2 of 0.427 (RMSE = 0.925°C; MAE = 0.576°C), whereas the nighttime model achieved an R^2 of 0.589 (RMSE = 0.359°C; MAE = 0.304°C). These results indicate moderate predictive performance, with the selected environmental variables explaining a greater proportion of the observed nighttime SUHI variability than the daytime variability under the random split. However, performance declined under the additional validation schemes. Temporal validation, using observations from 2000–2018 for training and 2019–2024 for testing, yielded R^2 values of 0.124 for daytime SUHI and 0.047 for nighttime SUHI. Leave-one-city-out validation produced pooled R^2 values of −0.417 and −0.537 for daytime and nighttime SUHI, respectively. The negative R^2 values indicate that predictions for the held-out cities were less accurate, in terms of squared error, than predictions based on the mean of the pooled observed test values. These results demonstrate the results are true for cities considered and do not transfer to unseen cities. Consequently, the RF–SHAP findings are interpreted as exploratory, model-dependent predictive attributions rather than causal estimates of individual environmental effects. Random Forest provides a flexible framework for modelling nonlinear relationships between predictors and response variables (Breiman, 2001); however, the validation results indicate that the predictive relationships identified here should not be assumed to generalize consistently across time or to other cities.

The pairwise Pearson correlation analysis revealed varying degrees of association among the four urban–rural predictor contrasts (Table S3). The strongest correlation was observed between ΔNDVI and ΔNDBI (r=-0.699), followed by ΔNDVI and ΔAOD (r=-0.486) and ΔNDBI and ΔAOD (r=0.493). Correlations between ΔNDVI and ΔAlbedo, ΔNDBI and ΔAlbedo, and ΔAOD and ΔAlbedo were −0.157, 0.457, and 0.392, respectively. These associations indicate that the predictors share some statistical information and should not necessarily be interpreted as independent environmental signals.

The VIF analysis further indicated potential linear redundancy among the predictors (Table S4). ΔNDVI had the highest VIF (11.29), followed by ΔAlbedo (7.13), ΔNDBI (4.48), and ΔAOD (3.15). The elevated VIF values for ΔNDVI and ΔAlbedo suggest appreciable redundancy in the pooled predictor dataset. However, VIF is an exploratory diagnostic of linear predictor dependence and does not directly assess the predictive validity of Random Forest models. These results were therefore considered when interpreting individual SHAP contributions, particularly where predictors may share predictive information.

Temporal autocorrelation was examined by removing the linear trend from each city-specific annual series and calculating lag-1 correlations between residuals from consecutive years (Table S5). Positive residual autocorrelation was observed for daytime SUHI in Rajkot ((r=0.411)) and ΔAOD in Ahmedabad ((r=0.410)) and Gandhinagar

((r=0.434)). However, none of the 30 city-by-variable tests remained statistically significant after Benjamini–Hochberg adjustment for multiple comparisons. Given the limited length of the annual series, these results should be interpreted cautiously and do not establish that the observations are temporally independent.

Because both SUHI and the indicators (ΔNDVI, ΔNDBI, ΔAOD, and ΔAlbedo) are expressed as urban–rural contrasts, their relationships may partly reflect shared land-surface transformation processes rather than independent environmental effects. Furthermore, pooling annual observations from five cities does not explicitly separate within-city temporal variability from between-city differences. Despite temporal and leave-one-city-out validation, the limited predictive performance indicates restricted generalizability across periods and cities. Temporal autocorrelation, common trends, and city-specific effects therefore remain potential sources of uncertainty. Future studies could employ panel-data or hierarchical modelling approaches to better distinguish temporal variations from city-specific effects and account for dependence among repeated observations.

3.5.2. *SHAP-based attribution of surface urban heat island variability*

SHapley Additive exPlanations (SHAP) analysis was applied to the city-specific RF models for Ahmedabad, Gandhinagar, Rajkot, Surat, and Vadodara to examine the relative predictive attributions of ΔNDVI, ΔNDBI, ΔAOD, and ΔAlbedo for daytime and nighttime SUHI predictions (Figure 8). Mean absolute SHAP values were normalized and expressed as percentages to facilitate comparisons among predictors, cities, and diurnal periods (Chakraborty & Lee, 2019; Lundberg & Lee, 2017). These percentages represent each predictor's share of the summed absolute SHAP attribution within the corresponding city-specific model; they do not represent the percentage of SUHI explained by an

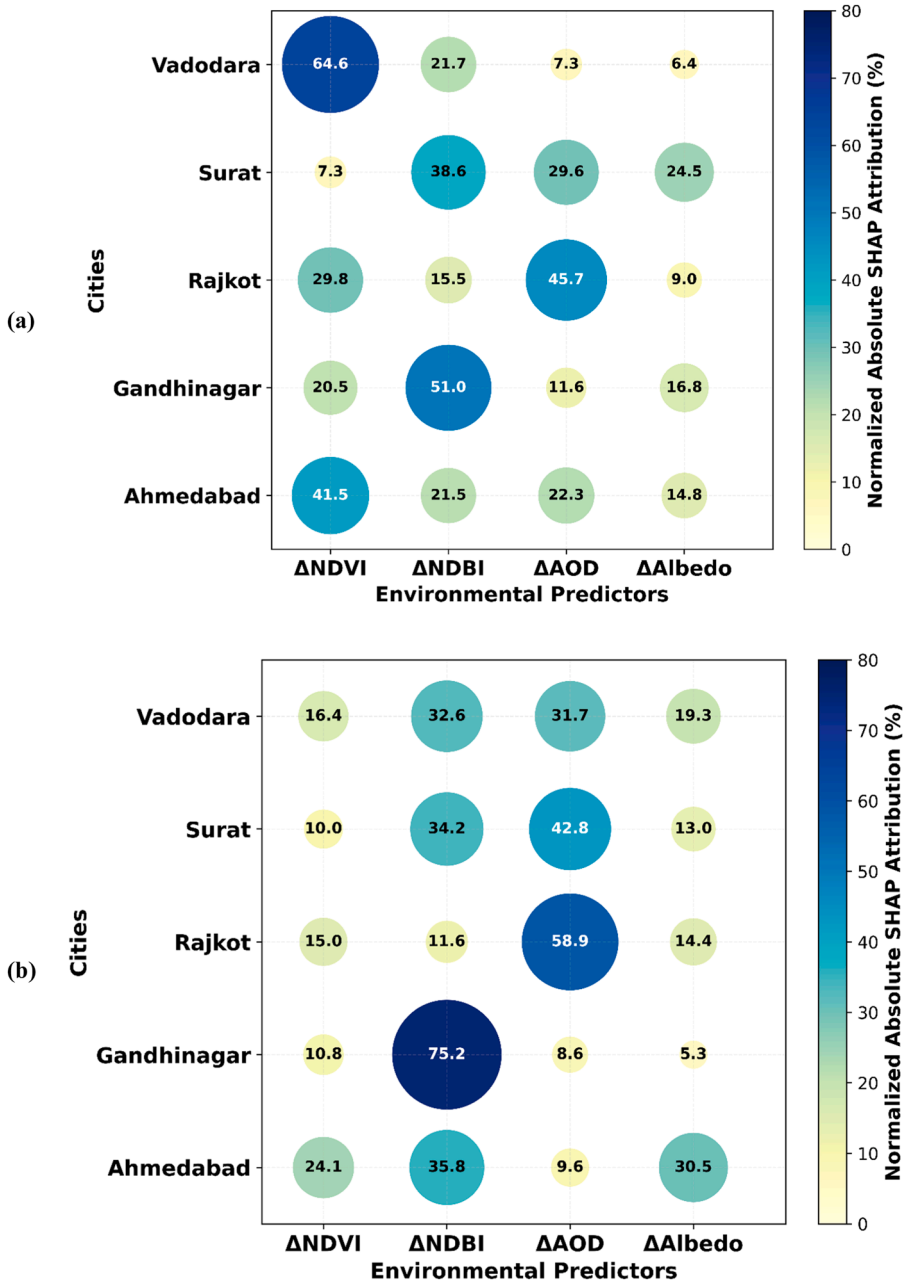

Fig. 8. City-Wise Random Forest–SHAP Attribution of Intra-City Surface Urban Heat Island (SUHI)Intensity to Δ Environmental differences (Urban-Rural): (a) Daytime and (b) Nighttime Conditions Across Gujarat Cities, India. ***Bubble size and colour represent the normalized mean absolute SHAP contribution (%), indicating the relative predictive importance of each variable within the corresponding fitted city-specific model.***

individual predictor or its causal contribution. Because the predictors may be interrelated and share predictive information, their individual attributions should not be interpreted as independent environmental effects. Furthermore, each city-specific model was fitted using 25 annual observations without independent held-out validation; consequently, the resulting attribution percentages are interpreted as exploratory, model-dependent summaries rather than robust estimates of predictor effects.

The daytime SHAP results revealed spatial heterogeneity in the normalized absolute SHAP attribution profiles of the selected environmental variables (Fig. 8a). ΔNDVI accounted for 41.5% and 64.6% of the normalized absolute SHAP attribution in the Ahmedabad and Vadodara daytime models, respectively, whereas ΔNDBI accounted for 51.0% and 38.6% in the Gandhinagar and Surat daytime models, respectively. In Rajkot, ΔAOD represented the largest attribution share, at 45.7%. Secondary attribution shares were also notable: ΔNDVI represented 20.5% and 29.8% of the normalized absolute SHAP attribution in the Gandhinagar and Rajkot daytime models, respectively, while ΔAOD represented 29.6% and ΔAlbedo 24.5% in the Surat daytime model. These results indicate that the relative magnitudes of model-specific predictor attributions varied across cities. The prominence of vegetation and built-up characteristics in some city-specific models is consistent with previous remote-sensing and machine-learning research examining relationships between land cover and SUHI variability (Chakraborty et al., 2020; Ghosh et al., 2022; Sethi & Vinoj, 2024; Singh et al., 2022). This consistency provides context for the observed predictive associations but does not establish causal effects.

During nighttime (Fig. 8b), ΔNDBI accounted for 35.8%, 75.2%, and 32.6% of the normalized absolute SHAP attribution in the Ahmedabad, Gandhinagar, and Vadodara models, respectively. ΔAOD showed the largest attribution share in the Rajkot and Surat models, at 58.9% and 42.8%, respectively. Other predictors also exhibited substantial attribution shares in selected cities, including ΔAlbedo in Ahmedabad (30.5%) and ΔAOD in Vadodara (31.7%). These values indicate differences in the relative attribution patterns across the fitted city-specific models. However, given the observed multicollinearity among predictors, particularly the elevated VIF values for ΔNDVI (11.29) and ΔAlbedo (7.13), these attribution shares should be interpreted cautiously. They represent model-dependent predictive attributions rather than independent contributions or causal effects of individual environmental variables. The patterns can be considered alongside previous research on urban land cover, morphology, atmospheric conditions, and surface energy exchange in urban thermal environments (Li et al., 2011; Zhao et al., 2014). However, the attribution rankings do not establish the physical mechanisms responsible for these relationships or quantify the independent effects of the predictors.

To complement the attribution rankings, signed SHAP values were examined to assess the direction of the fitted predictor–response relationships (Supplementary Figure S1). In the pooled daytime model, higher values of ΔAOD and ΔNDBI were generally associated with positive SHAP values, whereas lower ΔAOD values were associated predominantly with negative SHAP values. The daytime ΔNDVI distribution also showed predominantly positive SHAP values at higher predictor values. In contrast, the pooled nighttime model showed a different pattern for ΔNDVI and ΔAOD: higher ΔNDVI values were predominantly associated with negative SHAP values, while lower values were associated with positive SHAP values; higher ΔAOD values likewise tended to correspond to negative SHAP values. These patterns indicate that the direction of model-predicted associations differed between daytime and nighttime conditions. They describe the behaviour of the fitted pooled models and should not be interpreted as causal effects or as uniform relationships within every city.

City-specific SHAP dependence plots further revealed variation in the direction and shape of predictor–response patterns across the five cities (Supplementary Figures S2a and S2b). For daytime ΔNDVI, Ahmedabad, Rajkot, and Vadodara showed predominantly negative SHAP values at lower predictor values and positive values at higher predictor values, whereas Gandhinagar displayed a comparatively weak pattern around zero and Surat showed a more limited range of SHAP responses. The daytime ΔNDBI patterns also differed among cities: Ahmedabad, Surat, and Vadodara showed predominantly negative SHAP values at higher ΔNDBI values, while Gandhinagar and Rajkot exhibited different, generally more positive patterns over parts of their observed ranges. These contrasting patterns indicate that the pooled relationships do not fully represent the variation among city-specific models. Nevertheless, the limited sample size and possible predictor dependence prevent these patterns from being interpreted as stable city-specific physical responses.

The nighttime dependence plots likewise showed heterogeneous patterns (Supplementary Figure S2b). The relationship between ΔNDVI and signed SHAP values was generally negative across several city-specific models, although the magnitude and distribution of SHAP values varied among cities. For ΔNDBI, the patterns differed in direction and spread, with more pronounced negative SHAP values over parts of the observed range in Gandhinagar, Surat, and Vadodara. The nighttime ΔAOD relationships also varied: Rajkot showed predominantly positive SHAP values at lower ΔAOD values and negative values over much of the higher range, whereas Surat exhibited a contrasting pattern, with negative SHAP values at lower ΔAOD values and positive values over part of the higher range. The separate cross-city comparison of nighttime ΔAOD (Supplementary Figure S3) further illustrates this heterogeneity, including differences in the sign and spread of SHAP values among cities. These patterns suggest that aerosol-related predictive associations were not uniform across the fitted city-specific models; however, they do not establish the underlying atmospheric or surface-energy mechanisms.

The pooled accumulated local effects (ALE) plots provide a complementary representation of the fitted models' responses to the four predictors under daytime and nighttime conditions (Supplementary Figure S4). The curves display different response shapes across predictors and diurnal periods, including relatively abrupt changes in some daytime relationships and a declining nighttime response for ΔNDVI and ΔAOD over parts of their observed ranges. These features suggest potential nonlinearities in the fitted models. However, the abrupt changes, limited number of observations, and sensitivity of ALE estimates to binning warrant caution. Accordingly, the ALE curves are used as exploratory descriptions of model behaviour rather than evidence of physical thresholds or causal responses.

Overall, the RF–SHAP analysis revealed differences in normalized absolute SHAP attribution profiles between daytime and nighttime conditions and across the five Gujarat cities. ΔNDVI represented the largest attribution share in the Ahmedabad and Vadodara daytime models, whereas ΔNDBI represented the largest share in the Gandhinagar and Surat daytime models. At night, ΔNDBI represented the largest attribution share in the Ahmedabad, Gandhinagar, and Vadodara models, whereas ΔAOD represented the largest share in the Rajkot and Surat models. The signed SHAP and dependence analyses additionally indicate that the direction and shape of the fitted predictor–response relationships can differ between diurnal periods and among cities. These patterns indicate that the relative predictive attribution of environmental variables was not uniform across cities or diurnal periods. They can inform city-specific hypotheses for further investigation; however, the SHAP rankings should not be interpreted as direct measures of mitigation potential or as evidence that modifying the highest-ranked predictor would necessarily produce the greatest reduction in SUHI. Assessing mitigation effectiveness would require additional analyses designed to evaluate specific interventions.

3.6. Spatial patterns of urban thermal intensification and environmental change

Fig. 9(a–b) illustrates the spatial patterns of temporal changes (ΔLST_t, $\Delta SUHI_t$, ΔAOD_t, $\Delta NDVI_t$, and $\Delta NDBI_t$) across the five Gujarat

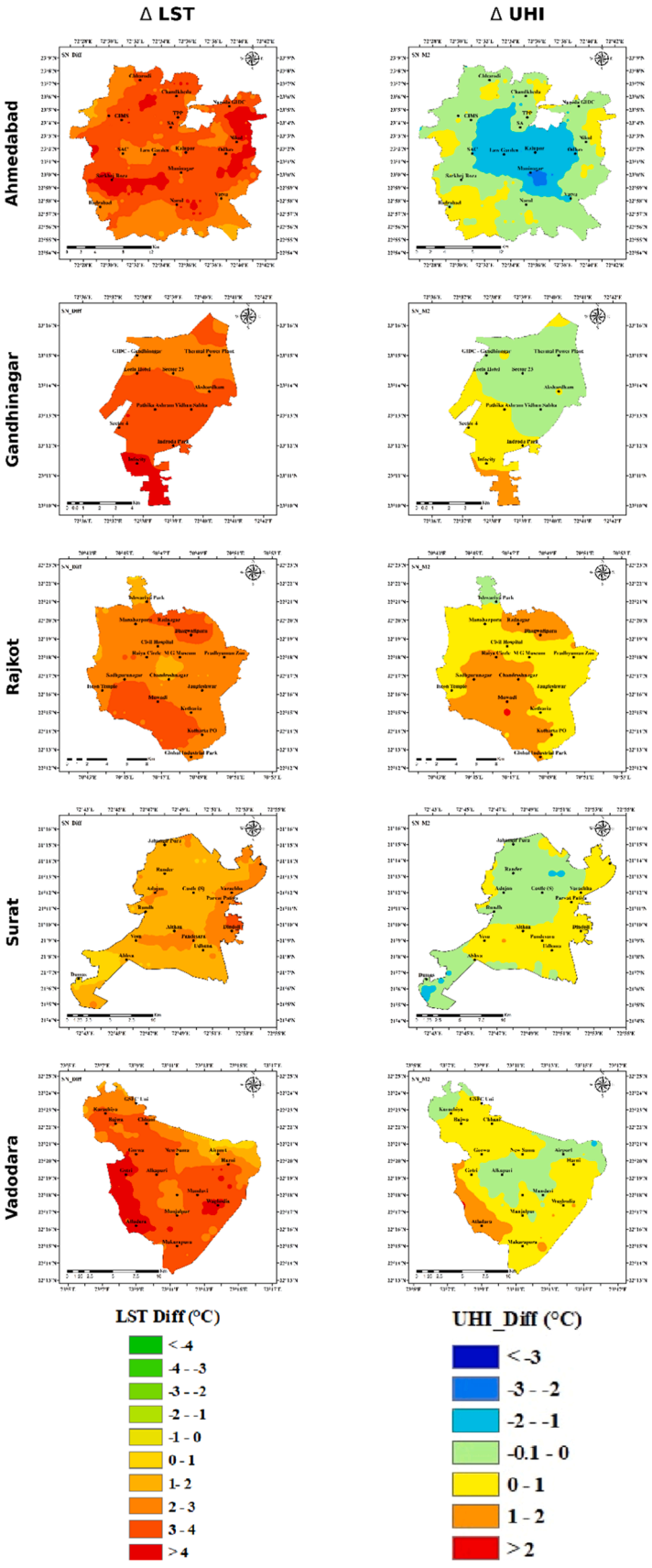

Fig. 9. (a) Spatial changes in ΔLST_t and $\Delta SUHI_t$ across five cities of Gujarat (2001–2024). (b) Spatial changes in ΔAOD_t, $\Delta NDVI_t$, and $\Delta NDBI_t$ across five cities of Gujarat (2001–2024).

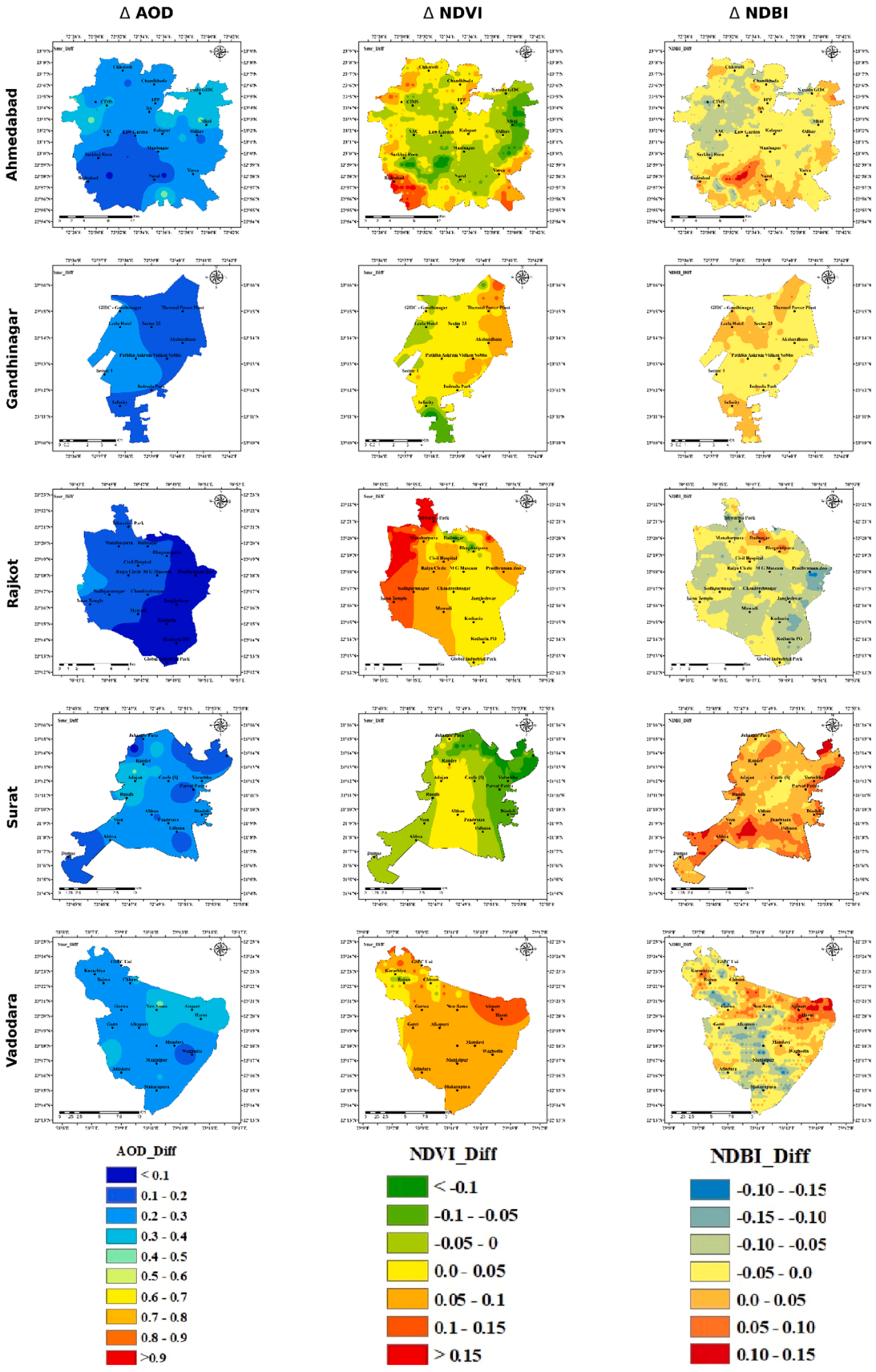

Fig. 9. (*continued*).

cities during 2001–2024, highlighting the spatial correspondence between changes in surface thermal conditions and changes in environmental indicators. To complement the visual comparison, spatial correlation analysis was used to quantify the relationships between

thermal changes (ΔLST_t and $\Delta SUHI_t$) and environmental changes ($\Delta NDVI_t$, $\Delta NDBI_t$, and ΔAOD_t). The analysis evaluates whether locations exhibiting greater thermal changes also tend to exhibit greater changes in vegetation, built-up intensity, or aerosol loading. Previous studies have reported associations between urban thermal patterns, land-cover transformation, and urban expansion, particularly in areas experiencing vegetation loss and increasing impervious surfaces (Ghosh et al., 2022; Li & Gao, 2025; Peng et al., 2012).

Ahmedabad exhibited widespread surface warming, with ΔLST_t increases of approximately +2 to +4°C across much of the study area and localized hotspots exceeding +4°C in the eastern and southeastern urban corridors, including Naroda, Odhav, Vatva, Nikol, and Kathwada (Fig. 9a). These warming zones spatially coincided with vegetation decline and increasing built-up intensity (Fig. 9b). This spatial correspondence is consistent with previously reported associations between land-cover characteristics and urban thermal patterns in rapidly urbanizing Indian cities (Guha et al., 2018; Sethi & Vinoj, 2024), although the present spatial comparison does not establish the causal contribution of individual factors. Although $\Delta SUHI_t$ increases were generally moderate (0–1°C), the mapped patterns indicate that surface warming was spatially extensive. The distinction between ΔLST_t and $\Delta SUHI_t$ is important because an increase in surface temperature does not necessarily imply an equivalent increase in the urban–rural temperature difference.

Gandhinagar displayed comparatively moderate surface warming, primarily within the +1 to +3°C range, accompanied by limited $\Delta SUHI_t$ enhancement (Fig. 9a). Localized hotspots occurred in southern and peripheral urban expansion zones, while substantial portions of the city retained relatively stable vegetation cover (Fig. 9b). These spatial patterns coincided with a comparatively small urban–rural built-up contrast, although the spatial comparison alone cannot establish that vegetation persistence or limited built-up expansion caused the weaker thermal response.

Rajkot experienced moderate surface warming (+1 to +3°C) and comparatively weak SUHI intensification (Fig. 9a). Vegetation decline was particularly evident across western and northwestern sectors, while built-up expansion appeared relatively limited in the mapped contrasts (Fig. 9b). These patterns indicate that the spatial extent of environmental change and the magnitude of thermal change did not necessarily vary proportionally. The observed correspondence does not, by itself, identify the processes responsible for the comparatively weaker thermal amplification.

Surat exhibited substantial environmental transformation, characterized by extensive warming (+2 to +4°C) and localized $\Delta SUHI_t$ increases approaching +1–2°C (Fig. 9a). The strongest hotspots occurred within eastern and northeastern urban growth corridors, where increases in built-up intensity coincided spatially with persistent vegetation deficits (Fig. 9b). These patterns are consistent with associations between land-cover transformation and urban thermal variability reported in previous studies. However, the spatial concurrence does not independently quantify the effects of urban expansion or industrial development on hotspot formation.

Vadodara showed extensive surface warming, with several southwestern and central sectors exceeding +3 to +4°C and some of the strongest localized $\Delta SUHI_t$ increases among the five cities (Fig. 9a). These hotspots coincided with areas of declining vegetation and increasing impervious-surface intensity (Fig. 9b). The observed spatial correspondence is consistent with established relationships between land-cover characteristics and urban thermal conditions, although the individual contributions of heat storage and evapotranspiration were not directly quantified in this analysis.

Across the five cities, the mapped ΔAOD_t patterns indicated changes in aerosol contrast, with positive values predominantly within the 0.1–0.5 range and larger increases reported in Ahmedabad, Surat, and Vadodara (Fig. 9b). In most cities, thermal hotspots appeared more spatially aligned with $\Delta NDVI_t$ and $\Delta NDBI_t$ patterns than with ΔAOD_t. This spatial correspondence is consistent with previous research examining land-cover transformation, aerosol loading, and SUHI variability (Chakraborty et al., 2020; Du et al., 2023; Mohammad & Goswami, 2021). Recent studies further indicate that aerosol–thermal relationships are spatially heterogeneous and may involve interactions with radiation and vegetation (Zou et al., 2025).

The quantitative spatial analysis revealed city-specific relationships between thermal and environmental changes across the five cities (Fig. 9). ΔLST_t was negatively associated with $\Delta NDVI_t$ in Ahmedabad ($r = -0.344$), Gandhinagar ($r = -0.286$), Surat ($r = -0.381$), and Vadodara ($r = -0.255$), whereas the association was negligible in Rajkot ($r = -0.027$). The corresponding $\Delta SUHI_t$–$\Delta NDVI_t$ association was strongest in Surat ($r = -0.504$), followed by Ahmedabad ($r = -0.386$), Gandhinagar ($r = -0.332$), Vadodara ($r = -0.308$), and Rajkot ($r = -0.025$). Associations between ΔLST_t and $\Delta NDBI_t$ were positive in Ahmedabad ($r = 0.479$), Gandhinagar ($r = 0.194$), Rajkot ($r = 0.244$), and Surat ($r = 0.217$), but negative in Vadodara ($r = -0.350$). Similarly, $\Delta SUHI_t$ was positively associated with $\Delta NDBI_t$ in Ahmedabad ($r = 0.505$), Gandhinagar ($r = 0.182$), Rajkot ($r = 0.330$), and Surat ($r = 0.198$), but negatively associated in Vadodara ($r = -0.315$). Relationships involving ΔAOD_t also varied geographically. ΔLST_t was negatively associated with ΔAOD_t in Ahmedabad ($r = -0.449$), Rajkot ($r = -0.340$), Surat ($r = -0.312$), and Vadodara ($r = -0.026$), but positively associated in Gandhinagar ($r = 0.447$). The corresponding $\Delta SUHI_t$–ΔAOD_t correlations were negative in Ahmedabad ($r = -0.437$), Rajkot ($r = -0.334$), Surat ($r = -0.296$), and Vadodara ($r = -0.203$), but positive in Gandhinagar ($r = 0.294$). The correlations indicate that spatial relationships between thermal changes and environmental changes were heterogeneous across the five cities, with no uniform relationship across all locations and predictors. These results represent spatial associations rather than independent causal effects and should be interpreted cautiously because of differences in spatial resolution and data coverage, particularly the limited AOD sampling, and the potential influence of spatial autocorrelation.

Overall, the spatial comparison reveals city-specific correspondence among ΔLST_t, $\Delta SUHI_t$, $\Delta NDVI_t$, and $\Delta NDBI_t$. The patterns are consistent with established associations between vegetation, built-up characteristics, and urban thermal variability (Bowler et al., 2010; Chakraborty & Lee, 2019; Ghosh et al., 2022; Guha et al., 2018; Li et al., 2011; Sethi & Vinoj, 2024; Weng et al., 2004; Zhao et al., 2018). Nevertheless, spatial correspondence alone does not establish causation or demonstrate that vegetation loss and built-up expansion were the dominant independent causes of thermal hotspot development. The relative predictive contributions of the environmental variables are considered separately in the regression and RF–SHAP analyses.

4. Discussion and conclusion

This study identifies contrasting daytime and nighttime land surface temperature (LST) trends across five major cities of Gujarat during 2000–2024, alongside substantial inter-city differences in surface urban heat island (SUHI) intensity and temporal evolution. The combined evidence from urban–rural thermal contrasts, spatial analysis, and machine-learning attribution indicates that vegetation, built-up characteristics, and aerosol loading were associated with urban thermal variability, although their relative predictive contributions differed among cities and between daytime and nighttime conditions. These findings are consistent with previous studies examining relationships between land-cover transformation and urban thermal environments (Chakraborty & Lee, 2019; Du et al., 2023; Guha et al., 2018; Li & Gao, 2025). Importantly, the results demonstrate that urban thermal evolution is not governed by a uniform regional response; instead, its magnitude, direction, and environmental associations vary across cities and between daytime and nighttime conditions.

A key finding is the contrasting long-term behaviour of daytime and nighttime LST. Daytime LST declined in all five cities, with Sen's slopes

ranging from −0.066°C/year in Surat to −0.145°C/year in Rajkot. After autocorrelation adjustment and Benjamini–Hochberg (BH) correction, significant declines remained in Ahmedabad, Rajkot, Surat, and Vadodara, whereas the decline in Gandhinagar was not significant (Table S2). In contrast, nighttime LST increased in all five cities, with Sen's slopes ranging from +0.049°C/year in Gandhinagar to +0.108°C/year in Surat. Significant increases remained in Ahmedabad, Rajkot, Surat, and Vadodara, while Gandhinagar's trend was not significant (BH-adjusted $q = 0.2103$; Table S2). This day–night asymmetry indicates that urban surface thermal changes cannot be represented by a uniform warming trajectory. Differences in surface-energy partitioning, surface heat retention, and nocturnal cooling associated with urban materials and land-cover characteristics may help explain these contrasting patterns (Bhati & Mohan, 2018Liu et al., 2025; ; Oke, 1982; Stewart & Oke, 2012; Du et al., 2023). The coexistence of declining daytime LST and increasing nighttime LST highlights the importance of distinguishing diurnal thermal responses when evaluating long-term changes in urban surface temperatures. However, these trends alone do not establish changes in urban heat storage or the physical mechanisms governing nocturnal cooling.

Importantly, the temporal behaviour of SUHI differed from the absolute LST trends. Mean daytime SUHI was highest in Surat (3.80 ± 0.40°C) and Rajkot (3.30 ± 0.48°C), whereas Gandhinagar recorded the lowest mean (1.11 ± 0.18°C). At night, Surat (2.30 ± 0.23°C) and Vadodara (2.25 ± 0.24°C) recorded the highest mean SUHI, while Rajkot had a substantially lower value (0.62 ± 0.14°C) (Table S1). Despite relatively high nighttime SUHI in Surat and Vadodara, statistically significant nighttime intensification was observed only in Vadodara (+0.012°C/year, $p = 0.036$). Daytime SUHI also exhibited heterogeneous trends: significant decreases occurred in Ahmedabad (−0.048°C/year), Surat (−0.030°C/year), and Vadodara (−0.030°C/year), whereas Gandhinagar showed a significant increase (+0.013°C/year); Rajkot exhibited a nonsignificant decrease (−0.022°C/year) (Table S2). These results demonstrate that higher mean SUHI intensity does not necessarily indicate stronger long-term intensification. Since SUHI represents an urban–rural temperature difference, its temporal behaviour depends on changes in both urban and surrounding reference surfaces, rather than urban LST alone. Similar weak or negative daytime SUHI trends and contrasting day–night thermal patterns have been reported in other Indian cities (Mathew et al., 2018; More & Dhaarna, 2026). A central implication is that increasing nighttime LST does not necessarily translate into increasing nighttime SUHI, because the thermal evolution of the surrounding rural reference surface also contributes to the observed urban–rural contrast. This divergence between absolute LST trends and SUHI trends represents an important distinction in assessing long-term urban thermal change.

The contrasting thermal profiles of Rajkot and Vadodara further illustrate this spatial heterogeneity. Rajkot exhibited relatively high daytime SUHI (3.30 ± 0.48°C) but low nighttime SUHI (0.62 ± 0.14°C), whereas Vadodara recorded lower daytime SUHI (1.45 ± 0.31°C) and higher nighttime SUHI (2.25 ± 0.24°C). Rajkot also recorded the highest coefficient of variation in nighttime SUHI (22.05%), compared with the lowest value in Ahmedabad (7.96%) (Table S1). These differences suggest that local urban morphology, land-cover characteristics, and climatic settings may be associated with distinct diurnal thermal responses. The contrasting daytime–nighttime SUHI magnitudes in Rajkot and Vadodara demonstrate that cities within the same regional climatic setting can exhibit substantially different diurnal thermal profiles. This reversal in relative thermal intensity also indicates that a single daytime or nighttime indicator may not adequately represent the overall urban thermal characteristics of a city. Consequently, regional assessments should account for city-specific thermal behaviour rather than assume a uniform urban heat island response across Gujarat. Previous studies have similarly documented spatial variations in urban thermal conditions across Indian cities and other geographical settings (Li & Gao, 2025; Mohammad & Goswami, 2021; Sethi & Vinoj, 2024; Ye et al., 2026).

Seasonal distributions provide further evidence of diurnal and intercity differences. Daytime SUHI was generally highest during summer, with median values approaching 5°C in Surat, approximately 4°C in Rajkot, and 3.3°C in Ahmedabad, while Gandhinagar and Vadodara generally exhibited lower intensities. Nighttime SUHI distributions were comparatively compact, with median values of approximately 2.4–2.7°C in Surat and Vadodara, around 2.2°C in Ahmedabad, and 0.5–0.6°C in Rajkot (Fig. 4). The generally lower SUHI contrasts during the monsoon indicate seasonal variation in urban–rural thermal differences. These seasonal patterns are consistent with the influence of changing moisture availability, cloud conditions, atmospheric stability, and surface characteristics on urban thermal environments, although their individual contributions were not quantified in this study (Mohammad & Goswami, 2021; Peng et al., 2012; Siddiqui et al., 2021). The seasonal results further indicate that the magnitude of urban–rural thermal contrasts is dependent on both the season and the time of satellite observation. In particular, the stronger summer daytime contrasts in Surat and Rajkot identify these cities as having comparatively pronounced seasonal daytime surface thermal differences.

The spatial analysis further indicates that relationships between thermal change and environmental change vary across the five cities. Vegetation, built-up characteristics, and aerosol contrasts did not exhibit uniform associations with thermal changes, supporting a city-specific interpretation. Similarly, the RF–SHAP analysis identified differences in the relative predictive contributions of environmental variables between cities and day–night conditions. During daytime, ΔNDVI showed the largest normalized absolute SHAP attribution in Vadodara (64.6%) and a substantial attribution in Ahmedabad (41.5%), whereas ΔNDBI showed the largest attribution in Gandhinagar (51.0%) and Surat (38.6%). In Rajkot, ΔAOD exhibited the largest daytime attribution (45.7%). During nighttime, ΔNDBI showed the largest attribution in Ahmedabad (35.8%), Gandhinagar (75.2%), and Vadodara (32.6%), while ΔAOD had the largest attribution in Rajkot (58.9%) and Surat (42.8%). The importance of NDVI and NDBI in several city-specific models highlights the relevance of vegetation and built-up contrasts in explaining modelled SUHI variability, while the comparatively greater attribution of AOD in Rajkot and Surat indicates the need to consider city-specific aerosol conditions. These differences reveal that the relative predictive associations of environmental variables are neither spatially uniform nor consistent between daytime and nighttime conditions. However, these SHAP values represent model-dependent predictive attributions rather than independent or causal contributions, particularly where predictors are correlated. In addition, the normalized absolute SHAP percentages indicate relative attribution within each fitted model and should not be interpreted as percentages of SUHI explained or as independently quantified environmental effects. Previous explainable machine-learning studies have also identified vegetation and impervious surfaces as important predictors of SUHI variability, with differences between daytime and nighttime conditions (Fu et al., 2025; Ye et al., 2026).

From a planning perspective, these findings support consideration of urban vegetation conservation, urban greening, reflective and permeable surfaces, blue–green infrastructure, and climate-responsive urban design as components of heat adaptation. The observed city-specific thermal patterns reinforce the importance of tailoring heat-mitigation strategies to local land-cover and thermal characteristics rather than adopting identical interventions across all cities. The contrasting thermal profiles observed in Rajkot and Vadodara, together with the differences in environmental predictor attribution, suggest that urban heat adaptation should consider both daytime and nighttime thermal conditions and the specific characteristics of individual cities. Continuous satellite-based monitoring can support this process by identifying changing thermal patterns and environmental contrasts, contributing to urban resilience initiatives under India's Smart Cities Mission, the National Action Plan on Climate Change (NAPCC), and Heat Action Plan

frameworks. Nevertheless, the effectiveness of individual interventions requires separate evaluation through observational, experimental, or modelling approaches. In this context, long-term satellite monitoring can provide a useful screening framework for identifying locations and periods with pronounced surface thermal contrasts, while intervention-specific assessments are required to quantify actual cooling benefits.

Several limitations should be considered when interpreting these findings. The absence of explicit meteorological controls, including air temperature, precipitation, relative humidity, wind speed, incoming shortwave radiation, soil moisture, cloud cover, and boundary-layer height, limits the separation of land-surface influences from background climate variability. The use of fixed municipal boundaries and city-specific rural reference zones, without historical boundary updates, alternative buffer-distance sensitivity analysis, or elevation correction, may also influence urban–rural thermal contrasts. Furthermore, the 1-km spatial resolution of MODIS LST, differences in the native resolutions of satellite predictors, temporal compositing, and variations in valid observations introduce additional spatial and temporal uncertainties. Residual retrieval uncertainties associated with MODIS products may also affect the derived thermal and environmental estimates. The moderate predictive performance of the Random Forest models under the random 80:20 split (daytime $R^2 = 0.4273$; nighttime $R^2 = 0.5895$), together with substantially lower performance under temporal validation (daytime $R^2 = 0.124$; nighttime $R^2 = 0.047$) and leave-one-city-out validation (daytime $R^2 = -0.417$; nighttime $R^2 = -0.537$), requires cautious interpretation of SHAP attribution patterns as exploratory, model-dependent associations rather than independent causal contributions. The city-specific SHAP models, which were developed using 25 annual observations per city without independent held-out validation, should therefore be interpreted as exploratory, model-dependent assessments of relative predictive attribution. Predictor multicollinearity, particularly the relatively high VIFs for ΔNDVI (11.29) and ΔAlbedo (7.13), may further influence the allocation of predictive attribution among correlated environmental variables. Trend estimates may also be influenced by interannual variability and the relatively short 25-year observation period. These uncertainties were not quantitatively propagated through the analytical framework. Finally, the analysis does not directly quantify surface-energy balance, anthropogenic heat flux, human heat exposure, population vulnerability, or associated health outcomes. Future research integrating meteorological reanalysis, improved spatial and temporal observations, historical urban boundaries, alternative rural-reference definitions, energy-balance assessments, and population-level indicators would provide a more comprehensive understanding of urban thermal dynamics and their implications for urban heat risk.

Overall, this study provides a long-term assessment of urban surface thermal dynamics across five major cities of Gujarat, revealing substantial differences in daytime and nighttime LST trends, SUHI intensity, and environmental associations. Daytime LST declined across all five cities, with statistically significant decreases in four cities, whereas nighttime LST increased in all five cities, with statistically significant increases in four. The contrasting behaviour of absolute LST and SUHI demonstrates that increasing nighttime surface temperatures do not necessarily translate into uniform nighttime SUHI intensification. Nighttime SUHI intensified significantly only in Vadodara, while daytime SUHI trends were city-specific, decreasing in Ahmedabad, Surat, and Vadodara but increasing in Gandhinagar. Furthermore, the city-specific patterns of vegetation, built-up characteristics, and aerosol-related predictive attributions highlight the heterogeneous nature of urban thermal environments. By integrating long-term LST and SUHI trends, seasonal and spatial comparisons, and RF–SHAP attribution, this study demonstrates that urban thermal evolution needs to be evaluated through multiple complementary indicators rather than a single measure of surface warming. The findings establish the importance of distinguishing absolute urban surface-temperature changes from relative urban–rural thermal contrasts and of recognising city-specific diurnal thermal behaviour. These findings emphasize the importance of city-specific thermal assessments rather than generalized assumptions about urban warming. Integrating long-term satellite observations with meteorological information and localized urban planning can strengthen the scientific basis for urban heat adaptation and climate-resilient development across Gujarat.

Open research

The datasets used in this study are publicly available. MODIS Land Surface Temperature (MOD11A2 Version 6.1), Vegetation Index (MOD13A2 Version 6.1), Surface Reflectance (MOD09A1 Version 6.1), Aerosol Optical Depth (MOD04_3K Version 6.1), and Surface Albedo (MCD43A3 Version 6.1) products were obtained through NASA Earthdata and Google Earth Engine. ERA5 reanalysis data were accessed through the European Centre for Medium-Range Weather Forecasts (ECMWF) Climate Data Store. Processed city-level datasets and derived indicators used in this study are available from the corresponding author upon reasonable request. The analysis scripts used for data processing and visualization are available from the corresponding author upon reasonable request.

Plain language summary (PLS)

This study examined changes in land surface temperature and urban heat island intensity across five major cities in Gujarat, India, from 2000 to 2024. Daytime and nighttime temperature trends differed across cities, indicating that urban surface warming was not uniform across the two periods. Nighttime land surface temperature increased significantly in four cities, whereas nighttime urban heat island intensity increased significantly only in Vadodara. This distinction shows that rising urban temperatures do not necessarily indicate an increasing temperature difference between urban and surrounding rural areas. Random Forest and SHAP analyses identified vegetation and built-up contrasts as important predictors of urban thermal variability in several cities, while aerosol contrasts showed relatively greater predictive contributions in Rajkot and Surat. These relationships varied across cities and between daytime and nighttime conditions. Urban greening and climate-sensitive planning may help modify surface thermal conditions; their effects on human thermal comfort and heat exposure require further assessment.

Funding

This research received no specific grant from any funding agency in the public, commercial, or not-for-profit sectors.

CRediT authorship contribution statement

Yagni Rami: Writing – review & editing, Writing – original draft, Visualization, Software, Methodology, Formal analysis, Data curation, Conceptualization. **TC Chakraborty:** Writing – review & editing, Validation.

Declaration of competing interest

The authors declare that they have no known competing financial interests or personal relationships that could have appeared to influence the work reported in this paper.

Acknowledgement

T.C. 's contribution was supported by the Biological and Environmental Research program of the U.S. Department of Energy (DOE) Office of Science through a DOE Early Career Award. Pacific Northwest National Laboratory is operated for the DOE by the Battelle Memorial Institute under contract DE-AC05-76RL01830.

Supplementary materials

Supplementary material associated with this article can be found, in the online version, at doi:10.1016/j.scs.2026.108122.

Data availability

Data will be made available on request.

References

Arnfield, A. J. (2003). Two decades of urban climate research: A review of turbulence, exchanges of energy and water, and the urban heat island. *International Journal of Climatology, 23*(1), 1–26. https://doi.org/10.1002/joc.859

Bhati, S., & Mohan, M. (2018). WRF-urban canopy model evaluation for the assessment of heat island and thermal comfort over an urban airshed in India under varying land use/land cover conditions. *Geoscience Letters, 5*(1). https://doi.org/10.1186/s40562-018-0126-7

Bowler, D. E., Buyung-Ali, L., Knight, T. M., & Pullin, A. S. (2010). Urban greening to cool towns and cities: A systematic review of the empirical evidence. *Landscape and Urban Planning, 97*(3), 147–155. https://doi.org/10.1016/j.landurbplan.2010.05.006

Breiman, L. (2001). Random forests. *Machine Learning, 45*(1), 5–32. https://doi.org/10.1023/A:1010933404324

Chakraborty, T., Hsu, A., Manya, D., & Sheriff, G. (2019). Disproportionately higher exposure to urban heat in lower-income neighborhoods: A multi-city perspective. *Environmental Research Letters, 14*(10), Article 105003. https://doi.org/10.1088/1748-9326/ab3b99

Chakraborty, T., Hsu, A., Manya, D., & Sheriff, G. (2020). A spatially explicit surface urban heat island database for the United States: Characterization, uncertainties, and possible applications. *ISPRS Journal of Photogrammetry and Remote Sensing, 168*, 74–88. https://doi.org/10.1016/j.isprsjprs.2020.07.021

Chakraborty, T., & Lee, X. (2019). A simplified urban-extent algorithm to characterize surface urban heat islands on a global scale and examine vegetation control on their spatiotemporal variability. *International Journal of Applied Earth Observation and Geoinformation, 74*, 269–280. https://doi.org/10.1016/j.jag.2018.09.015

Chakraborty, T., Sarangi, C., & Tripathi, S. N. (2017). Understanding diurnality and inter-seasonality of a sub-tropical urban heat island. *Boundary-Layer Meteorology, 163*(2), 287–309.

Chakraborty, T., Venter, Z. S., Qian, Y., & Lee, X. (2022). Lower urban humidity moderates outdoor heat stress. *AGU Advances, 3*(5), Article e2022AV000729. https://doi.org/10.1029/2022AV000729

Chakraborty, T. C., Sarangi, C., & Lee, X. (2021). Reduction in human activity can enhance the urban heat island: Insights from the COVID-19 lockdown. *Environmental Research Letters, 16*(5), Article 054060. https://doi.org/10.1088/1748-9326/abef8e

Cuthbert, M. O., et al. (2022). Global climate-driven trade-offs between the water retention and cooling benefits of urban greening. *Nature Communications, 13*, 5734. https://doi.org/10.1038/s41467-022-33488-4

Dey, S., & Di Girolamo, L. (2011). A climatology of aerosol optical and microphysical properties over the Indian subcontinent from 9 years (2000–2008) of Multi-angle Imaging SpectroRadiometer (MISR) data. *Journal of Geophysical Research: Atmospheres, 116*, Article D15204. https://doi.org/10.1029/2010JD014918

Didan, K. (2015). MOD13Q1 MODIS/Terra vegetation indices 16-day L3 global 250 m SIN grid V006. *NASA Land Processes Distributed Active Archive Center*. https://doi.org/10.5067/MODIS/MOD13Q1.006 [Data set].

Didan, K. (2021). *MODIS/Terra Vegetation Indices 16-Day L3 Global 1km SIN Grid V061* https://doi.org/10.5067/MODIS/MOD13A2.061.

Du, H., Zhan, W., Voogt, J., Bechtel, B., Chakraborty, T., Liu, Z., Hu, L., Wang, Z., Li, J., Fu, P., Liao, W., Luo, M., Li, L., Wang, S., Huang, F., & Miao, S. (2023). Contrasting trends and drivers of global surface and canopy urban heat islands. *Geophysical Research Letters, 50*(15), Article e2023GL104661. https://doi.org/10.1029/2023GL104661

Fu, H., Wen, J., Liu, Z., Li, J., Li, J., & Chen, Z. (2025). Contrasting frequency of global canopy and surface urban heat island. *Sustainable Cities and Society, 133*, Article 106857. https://doi.org/10.1016/j.scs.2025.106857

Ghosh, S., Kumar, D., & Kumari, R. (2022). Assessing spatiotemporal variations in land surface temperature and SUHI intensity with a cloud based computational system over five major cities of India. *Sustainable Cities and Society, 85*, Article 104060. https://doi.org/10.1016/j.scs.2022.104060

Gorelick, N., Hancher, M., Dixon, M., Ilyushchenko, S., Thau, D., & Moore, R. (2017). Google Earth Engine: Planetary-scale geospatial analysis for everyone. *Remote Sensing of Environment, 202*, 18–27. https://doi.org/10.1016/j.rse.2017.06.031

Government of India, & Ministry of Housing and Urban Affairs. (2015). *Smart Cities Mission: Statement and guidelines*. Government of India. https://smartcities.gov.in/.

Guha, S., Govil, H., Dey, A., & Gill, N. (2018). Analytical study of land surface temperature with NDVI and NDBI using Landsat 8 OLI and TIRS data in Florence and Naples city, Italy. *European Journal of Remote Sensing, 51*(1), 667–678. https://doi.org/10.1080/22797254.2018.1474494

Halder, B., Bandyopadhyay, J., & Banik, P. (2021). Monitoring the effect of urban development on urban heat island based on remote sensing and geo-spatial approach in Kolkata and adjacent areas, India. *Sustainable Cities and Society, 74*, Article 103186. https://doi.org/10.1016/j.scs.2021.103186

India Meteorological Department (IMD). (2026). *Heat wave guidance bulletin: April–May 2026*. Ministry of Earth Sciences, Government of India. https://mausam.imd.gov.in/pdfs/heatcolduser/heat_bulletin.pdf.

Jin, M., Dickinson, R. E., & Zhang, D. (2005). The footprint of urban areas on global climate as characterized by MODIS. *Journal of Climate, 18*(10), 1551–1565. https://doi.org/10.1175/JCLI3334.1

Knowlton, K., Kulkarni, S. P., Azhar, G. S., Mavalankar, D., Jaiswal, A., Connolly, M., Nori-Sarma, A., Rajiva, A., Dutta, P., Deol, B., Sanchez, L., Khosla, R., Webster, P. J., Toma, V. E., Sheffield, P., & Hess, J. J. (2014). Development and implementation of South Asia's first heat-health action plan in Ahmedabad (Gujarat, India). *International Journal of Environmental Research and Public Health, 11*(4), 3473–3492. https://doi.org/10.3390/ijerph110403473

Kotharkar, R., & Bagade, A. (2018). Evaluating urban heat island in the critical local climate zones of an Indian city. *Landscape and Urban Planning, 169*, 92–104. https://doi.org/10.1016/j.landurbplan.2017.08.009

Kumar, R., & Mishra, V. (2019). Decline in surface urban heat island intensity in India during heatwaves. *Environmental Research Communications, 1*(3), Article 031001. https://doi.org/10.1088/2515-7620/ab121d

Kumar, R., Mishra, V., Buzan, J., Kumar, R., Shindell, D., & Huber, M. (2017). Dominant control of agriculture and irrigation on urban heat island in India. *Scientific Reports, 7*, Article 14054. https://doi.org/10.1038/s41598-017-14213-2

Levy, R. C., Mattoo, S., Munchak, L. A., Remer, L. A., Sayer, A. M., Patadia, F., & Hsu, N. C. (2013). The Collection 6 MODIS aerosol products over land and ocean. *Atmospheric Measurement Techniques, 6*(11), 2989–3034. https://doi.org/10.5194/amt-6-2989-2013

Li, J., Song, C., Cao, L., Zhu, F., Meng, X., & Wu, J. (2011). Impacts of landscape structure on surface urban heat islands: A case study of Shanghai, China. *Remote Sensing of Environment, 115*(12), 3249–3263. https://doi.org/10.1016/j.rse.2011.07.008

Li, K., & Gao, S. (2025). Global patterns and drivers of summertime surface urban heat island cohesion. *Sustainable Cities and Society, 128*, Article 106470. https://doi.org/10.1016/j.scs.2025.106470

Liu, Z., Li, J., Wu, Y., Qin, C., & Liu, Y. (2025). Temporal trend of the frequency and maximum durations of surface urban heat islands over global cities. *Sustainable Cities and Society, 120*, Article 106141. https://doi.org/10.1016/j.scs.2025.106141

Lucht, W., Schaaf, C. B., & Strahler, A. H. (2000). An algorithm for the retrieval of albedo from space using semiempirical BRDF models. *IEEE Transactions on Geoscience and Remote Sensing, 38*(2), 977–998. https://doi.org/10.1109/36.841980

Lundberg, S. M., & Lee, S.-I. (2017). A unified approach to interpreting model predictions. In I. Guyon, U. V. Luxburg, S. Bengio, H. Wallach, R. Fergus, S. Vishwanathan, & R. Garnett (Eds.), *Advances in Neural Information Processing Systems*. Curran Associates, Inc, 30 https://proceedings.neurips.cc/paper/2017/hash/8a20a8621978632d76c43dfd28b67767-Abstract.html.

Mallick, J., Rahman, A., & Singh, C. K. (2013). Modeling urban heat islands in heterogeneous land surface and its correlation with impervious surface area by using night-time ASTER satellite data in highly urbanizing city, Delhi-India. *Advances in Space Research, 52*(4), 639–655. https://doi.org/10.1016/j.asr.2013.04.025

Martin, P., Baudouin, Y., & Gachon, P. (2015). An alternative method to characterize the surface urban heat island. *International Journal of Biometeorology, 59*(7), 849–861. https://doi.org/10.1007/s00484-014-0902-9

Mathew, A., Khandelwal, S., & Kaul, N. (2016). Spatial and temporal variations of urban heat island effect and the effect of percentage impervious surface area and elevation on land surface temperature: Study of Chandigarh city, India. *Sustainable Cities and Society, 26*, 264–277. https://doi.org/10.1016/j.scs.2016.06.018

Mathew, A., Khandelwal, S., & Kaul, N. (2018). Analysis of diurnal surface temperature variations for the assessment of surface urban heat island effect over Indian cities. *Energy and Buildings*. https://doi.org/10.1016/j.enbuild.2017.10.062

Mohammad, P., & Goswami, A. (2021). Quantifying diurnal and seasonal variation of surface urban heat island intensity and its associated determinants across different climatic zones over Indian cities. *GIScience & Remote Sensing, 58*(7), 955–981. https://doi.org/10.1080/15481603.2021.1940739

Mohan, M., Kandya, A., & Battiprolu, A. (2011). Urban heat island effect over National Capital Region of India: A study using the temperature trends. *Journal of Environmental Protection, 2*(4), 465–472. https://doi.org/10.4236/jep.2011.24054

Mohan, M., Kikegawa, Y., Gurjar, B. R., Bhati, S., Kandya, A., & Ogawa, K. (2012). Urban heat island assessment for a tropical urban airshed in India. *Atmospheric and Climate Sciences, 2*(2), 127–138. https://doi.org/10.4236/acs.2012.22014

Mohan, M., Kikegawa, Y., Gurjar, B. R., Bhati, S., & Kolli, N. R. (2012). Assessment of urban heat island effect for different land use–land cover from micrometeorological measurements and remote sensing data for megacity Delhi. *Theoretical and Applied Climatology, 112*(3–4), 647–658. https://doi.org/10.1007/s00704-012-0758-z

Mohan, M., Sati, A. P., & Bhati, S. (2020). Urban sprawl during five decadal period over National Capital Region of India: Impact on urban heat island and thermal comfort. *Urban Climate, 33*, Article 100647. https://doi.org/10.1016/j.uclim.2020.100647

More, P., & Dhaarna. (2026). Urban heat & cool island: Investigating Pune's (India) thermal dynamics using MODIS and Landsat 8–9 data. *Sustainable Cities and Society, 138*, Article 107174. https://doi.org/10.1016/j.scs.2026.107174

Nayak, S., Vinod, A., & Prasad, A. K. (2023). Spatial characteristics and temporal trend of urban heat island effect over major cities in India using long-term space-based MODIS land surface temperature observations (2000–2023). *Applied Sciences, 13*(24), Article 13323. https://doi.org/10.3390/app132413323

Oke, T. R. (1982). The energetic basis of the urban heat island. *Quarterly Journal of the Royal Meteorological Society, 108*(455), 1–24. https://doi.org/10.1002/qj.49710845502

Peng, S., Piao, S., Ciais, P., Friedlingstein, P., Ottle, C., Bréon, F.-M., Nan, H., Zhou, L., & Myneni, R. B. (2012). Surface urban heat island across 419 global big cities.

Environmental Science & Technology, 46(2), 696–703. https://doi.org/10.1021/es2030438

Ramachandran, S., Kedia, S., & Srivastava, R. (2012). Aerosol optical depth trends over different regions of India. *Atmospheric Environment, 49*, 338–347. https://doi.org/10.1016/j.atmosenv.2011.11.017

Ramanathan, V., Crutzen, P. J., Kiehl, J. T., & Rosenfeld, D. (2001). Aerosols, climate, and the hydrological cycle. *Science, 294*(5549), 2119–2124. https://doi.org/10.1126/science.1064034

Santamouris, M. (2014). Cooling the cities – A review of reflective and green roof mitigation technologies to fight heat island and improve comfort in urban environments. *Solar Energy, 103*, 682–703. https://doi.org/10.1016/j.solener.2012.07.003

Santamouris, M. (2015). Analyzing the heat island magnitude and characteristics in one hundred Asian and Australian cities and regions. *Science of the Total Environment, 512–513*, 582–598. https://doi.org/10.1016/j.scitotenv.2015.01.060

Schaaf, C. B., Gao, F., Strahler, A. H., Lucht, W., Li, X., Tsang, T., Strugnell, N. C., Zhang, X., Jin, Y., Muller, J.-P., Lewis, P., Barnsley, M., Hobson, P., Disney, M., Roberts, G., Dunderdale, M., Doll, C., d'Entremont, R. P., Hu, B., … Roy, D. (2002). First operational BRDF, albedo nadir reflectance products from MODIS. *Remote Sensing of Environment, 83*(1–2), 135–148. https://doi.org/10.1016/S0034-4257(02)00091-3

Sethi, S. S., & Vinoj, V. (2024). Urbanization and regional climate change-linked warming of Indian cities. *Nature Cities, 1*, 402–405. https://doi.org/10.1038/s44284-024-00074-0

Shreevastava, A., Rao, P. S. C., & McGrath, G. S. (2019). Emergent self-similarity and scaling properties of fractal intra-urban heat islets for diverse global cities. *Physical Review E, 100*(3), Article 032142. https://doi.org/10.1103/PhysRevE.100.032142. Article.

Siddiqui, A., Kushwaha, G., Nikam, B., Srivastav, S. K., Shelar, A., & Kumar, P. (2021). Analysing the day/night seasonal and annual changes and trends in land surface temperature and surface urban heat island intensity (SUHII) for Indian cities. *Sustainable Cities and Society, 75*, Article 103374. https://doi.org/10.1016/j.scs.2021.103374

Singh, P., Chaudhuri, A. S., Verma, P., Singh, V. K., & Meena, S. R. (2022). Earth observation data sets in monitoring of urbanization and urban heat island of Delhi, India. *Geomatics, Natural Hazards and Risk, 13*(1), 1762–1779. https://doi.org/10.1080/19475705.2022.2097452

Stewart, I. D., & Oke, T. R. (2012). Local climate zones for urban temperature studies. *Bulletin of the American Meteorological Society, 93*(12), 1879–1900. https://doi.org/10.1175/BAMS-D-11-00019.1

Sultana, S., & Satyanarayana, A. N. V (2019). Impact of urbanisation on urban heat island intensity during summer and winter over Indian metropolitan cities. *Environmental Monitoring and Assessment, 191*(Suppl. 3). https://doi.org/10.1007/s10661-019-7692-9

Venter, Z. S., Chakraborty, T., & Lee, X. (2021). Crowdsourced air temperatures contrast satellite measures of the urban heat island and its mechanisms. *Science Advances, 7*(22). https://doi.org/10.1126/sciadv.abb9569. eabb9569.

Vermote, E. (2015). *MOD09A1 MODIS/Terra surface reflectance 8-day L3 global 500 m SIN grid V006 [Data set]*. NASA EOSDIS Land Processes Distributed Active Archive Center. https://doi.org/10.5067/MODIS/MOD09A1.006

Voogt, J. A., & Oke, T. R. (2003). Thermal remote sensing of urban climates. *Remote Sensing of Environment, 86*(3), 370–384. https://doi.org/10.1016/S0034-4257(03)00079-8

Wan, Z., Hook, S., & Hulley, G. (2021). *MODIS/Terra Land Surface Temperature/Emissivity 8-Day L3 Global 1km SIN Grid V061 [Dataset]*. NASA Land Processes Distributed Active Archive Center. https://doi.org/10.5067/MODIS/MOD11A2.061. Date Accessed: 2026-06-15.

Weng, Q. (2009). Thermal infrared remote sensing for urban climate and environmental studies: Methods, applications, and trends. *ISPRS Journal of Photogrammetry and Remote Sensing, 64*(4), 335–344. https://doi.org/10.1016/j.isprsjprs.2009.03.007

Weng, Q., Lu, D., & Schubring, J. (2004). Estimation of land surface temperature–vegetation abundance relationship for urban heat island studies. *Remote Sensing of Environment, 89*(4), 467–483. https://doi.org/10.1016/j.rse.2003.11.005

Ye, F., Wang, S., & Li, X. (2026). Attributing the urban heat island effect to urban land use patterns with integrated machine learning and GeoShapley method. *Sustainable Cities and Society, 145*, Article 107457. https://doi.org/10.1016/j.scs.2026.107457

Zha, Y., Gao, J., & Ni, S. (2003). Use of normalized difference built-up index in automatically mapping urban areas from TM imagery. *International Journal of Remote Sensing, 24*(3), 583–594. https://doi.org/10.1080/01431160304987

Zhao, C., Jensen, J., Weng, Q., & Weaver, R. (2018). A geographically weighted regression analysis of the underlying factors related to the surface urban heat island phenomenon. *Remote Sensing, 10*(9), 1428. https://doi.org/10.3390/rs10091428

Zhao, L., Lee, X., Smith, R. B., & Oleson, K. (2014). Strong contributions of local background climate to urban heat islands. *Nature, 511*(7508), 216–219. https://doi.org/10.1038/nature13462

Zou, J., Chen, H. W., Li, H., Wang, Q., Wang, G., Jia, K., et al. (2025). Amplified urban heat island effect in southern China's old towns following atmospheric regulation policies. *Sustainable Cities and Society, 131*, Article 106675. https://doi.org/10.1016/j.scs.2025.106675